HHS Public Access

Author manuscript

Sci Signal. Author manuscript; available in PMC 2019 September 12.

Published in final edited form as:

Sci Signal. ; 12(572): . doi:10.1126/scisignal.aau4543.

Manganese promotes the aggregation and prion-like cell-to-cell exosomal transmission of α-synuclein

Dilshan S. Harischandra[1,†], **Dharmin Rokad**[1,‡], **Matthew L. Neal**[1,‡], **Shivani Ghaisas**[1], **Sireesha Manne**[1], **Souvarish Sarkar**[1], **Nikhil Panicker**[1], **Gary Zenitsky**[1], **Huajun Jin**[1], **Mechelle Lewis**[2], **Xuemei Huang**[2], **Vellareddy Anantharam**[1], **Arthi Kanthasamy**[1], and **Anumantha G. Kanthasamy**[1,*]

[1]Parkinson's Disorder Research Program, Iowa Center for Advanced Neurotoxicology, Department of Biomedical Sciences, Iowa State University, Ames, IA 50011.

[2]Departments of Neurology and Pharmacology, Pennsylvania State University-Milton S. Hershey Medical Center, Hershey, PA 17033.

Abstract

The aggregation of α-synuclein (αSyn) is considered a key pathophysiological feature of certain neurodegenerative disorders, collectively termed synucleinopathies. Given that a prion-like, cell-to-cell transfer of misfolded αSyn has been recognized in the spreading of αSyn pathology in synucleinopathies, we investigated the biological mechanisms underlying the propagation of the disease with respect to environmental neurotoxic stress. Considering the potential role of the divalent metal manganese (Mn^{2+}) in protein aggregation, we characterized its effect on αSyn misfolding and transmission in experimental models of Parkinson's disease. In cultured dopaminergic neuronal cells stably expressing wild-type human αSyn, misfolded αSyn was secreted through exosomes into the extracellular medium upon Mn^{2+} exposure. These exosomes were endocytosed through caveolae into primary microglial cells, thereby mounting neuroinflammatory responses. Furthermore, Mn^{2+}-elicited exosomes exerted a neurotoxic effect in a human dopaminergic neuronal model (LUHMES cells). Moreover, bimolecular fluorescence complementation (BiFC) analysis revealed that Mn^{2+} accelerated the cell-to-cell transmission of αSyn, resulting in dopaminergic neurotoxicity in a mouse model of Mn^{2+} exposure. Notably, welders exposed to Mn^{2+} had increased misfolded αSyn content in their serum exosomes. Stereotaxically delivering αSyn-containing exosomes, isolated from Mn^{2+}-treated αSyn-

*Corresponding author. akanthas@iastate.edu.

†Current affiliation: The Perelman School of Medicine, University of Pennsylvania, Philadelphia, PA, 19104.

‡These authors contributed equally to this work.

Author contributions:

D.S.H. and A.G.K. conceived and designed experiments. D.S.H., M.L.N., D.R., S.G., S.M., S.S., N.P. and G.Z. performed the experiments and analyzed the data. A.K, H.J. and V.A. provided intellectual input on experimental design, data analysis, interpretation and manuscript preparation. M.L. and X.H. provided key data regarding human samples (welder and controls) and assistance with the experimental design and interpretation, and review of the manuscript. D.S.H., H.J., G.Z. and A.G.K. wrote the manuscript and all authors reviewed and edited the manuscript.

Competing interests:

A.G.K. and V.A. have an equity interest in PK Biosciences Corporation located in Ames, IA. The terms of this arrangement have been reviewed and approved by Iowa State University in accordance with its conflict of interest policies. Other authors declare no competing financial interests.

Data and materials availability: All data needed to evaluate the conclusions in the paper are present in the paper or the Supplementary Materials. Any material in this manuscript may be obtained through an MTA.

expressing cells, into the striatum initiated Parkinsonian-like pathological features in mice. Together, these results indicate that Mn^{2+} exposure promotes αSyn secretion in exosomal vesicles, which subsequently evokes proinflammatory and neurodegenerative responses in both cell culture and animal models.

Introduction

Synucleinopathies are characterized by the presence of cytoplasmic inclusions called Lewy bodies and neurites composed of α-synuclein (αSyn) and ubiquitin (1). Among them, Parkinson's disease (PD) is the most common, marked by motor and non-motor deficits and progressive degeneration of dopaminergic neurons projecting from the substantia nigra pars compacta (SNpc) to the striatum. Multiple system atrophy (MSA) and diffuse Lewy body disease (DLB) also belong to this group of disorders, with Lewy bodies found primarily in glial cells of the basal ganglia in MSA and in more diffuse areas of the cortex in DLB. Although the physiological functions of αSyn are poorly understood, evidence suggests that the accumulation of aberrant αSyn species exerts intracellular toxic effects in the central nervous system (CNS). The idea that αSyn can pathologically propagate throughout the CNS recently gained much attention with the finding of αSyn species in human plasma and cerebral spinal fluid (CSF) (2, 3) and the host-to-graft propagation of αSyn-positive Lewy bodies in fetal ventral mesencephalic and embryonic nigral neurons transplanted in human PD patients (3, 4). Indeed, recent studies have suggested that intercellular transmission of αSyn aggregates is associated with the progression of PD (5–7) and MSA (8).

Accumulating evidence indicates that extracellular αSyn becomes pathogenic by activating neuroinflammatory and neurodegenerative responses *in vitro* (9, 10). The nature of the secretory mechanisms of αSyn remains elusive. However, studies have shown that neurons can secrete αSyn into the extracellular milieu through a brefeldin-A–insensitive pathway involving exosome vesicles (6, 11). Exosomes are nano-scale vesicles generated within the endosomal system and secreted upon fusion of multivesicular bodies with the plasma membrane. Originally, exosomes were thought to be molecular "garbage bags" associated with disposal of waste materials from cells. However, it was discovered that exosomes are more like molecular cargo vessels carrying key molecules that include miRNAs and proteins and, therefore, playing a role in cell-to-cell communication and disease propagation (9, 12–14). Thus, understanding exosome biology can advance therapeutic and biomarker discoveries in many diseases including neurological diseases.

Emerging evidence from many neurodegenerative disorders, including synucleinopathies, now has expanded the notion of cell-to-cell transmission of misfolded proteins as a common mechanism for the onset and progression of these diseases (15–18). Although the exact mechanisms for protein aggregate spreading in the CNS still largely remain unknown, several models including exocytosis, cell injury, receptor-mediated endocytosis, tunneling nanotubes, and exosomal transmission have been proposed (7). Although genetic predisposition is an important risk factor in many familial cases of Parkinsonian syndromes, environmental exposure to certain metals, herbicides, or insecticides has been linked to the pathogenesis of these diseases (19). This includes the divalent metal manganese (Mn) that

humans are exposed to through contaminated air and drinking water, as well as the use of Mn-containing consumer and agricultural products. In trace amounts, Mn is essential for human health, but environmental exposure to high doses of Mn results in manganism, a debilitating movement disorder sharing many Parkinsonian features, although it may not represent clinical PD, because manganism lacks the classic response to levodopa and certain distinctive neurological symptoms (20). Occupational exposure Mn containing welding fumes has been linked increased risk of Parkinsonism (21–24). Yet, despite its prevalence and thus potential risk to human health and the development of neurodegenerative disorders, the mechanisms by which Mn exerts its neurotoxic effects and its role in the prion-like propagation of αSyn aggregates are not well understood thus far.

Hence, in this study we assessed the effects of environmental Mn on αSyn aggregation, secretion, and cell-to-cell transmission. To elucidate the mechanism of Mn-induced αSyn release, we followed a systematic approach from in vitro to ex vivo and finally in vivo experimental models as well as human samples to better understand the role of exosomes in cell-to-cell transmission of misfolded αSyn protein.

Results

Mn exposure upregulates oligomeric αSyn secretion in exosomes

Emerging evidence indicates that misfolded αSyn is a transmissible pathological agent responsible for the initiation and spread of Parkinsonian pathology (25–27). To investigate the effect of exposure to the neurotoxic metal Mn on αSyn transmission and the underlying molecular mechanisms, we established an αSyn-expressing dopaminergic neuronal cell model (GFP_Syn) by stably transfecting MN9D mouse dopaminergic neuronal cells with a construct encoding amino-terminal GFP-tagged human wild-type (WT) αSyn. A control cell line (GFP_EV) also was generated by stably transfecting cells with a pmaxFP-Green-N control vector. Immunocytochemical analyses indicated that >90% of the GFP_Syn cells were positive for GFP-tagged human αSyn, and that all GFP_EV cells were positive for GFP (Fig. 1A). Western blots indicated a low abundance of endogenous αSyn in both stable cell lines and a greater abundance of GFP-tagged αSyn in GFP_Syn cells (Fig. 1B).

Next, we performed 3-(4, 5-dimethylthiazolyl-2)-2, 5-diphenyltetrazolium bromide (MTT)-based cytotoxicity assays to determine the sensitivity of naïve MN9D cells to Mn. The Mn concentration required to kill 50% of MN9D cells (LC_{50}) in 24 hours was 1129 μM (Fig. S1A). Based on this LC_{50} and previously published doses for Mn in dopaminergic neuronal cell lines (28, 29), we chose to use a low dose, 300 μM, Mn for our subsequent studies. To evaluate whether αSyn was released from the cells, we analyzed the amount of secreted αSyn in the conditioned media after Mn treatment in serum-free DMEM. The medium was collected and concentrated using centrifugal concentrators together with BSA (10 μg/ml final concentration) as an internal spiked control. Mn treatment at 300 μM markedly enhanced the release of GFP-tagged αSyn into the extracellular milieu when compared to time-matched untreated cells (Fig. 1C, S1B). We also immunoblotted the same membranes with an antibody against lactate dehydrogenase A (LDHA), an enzyme marker indicative of cellular toxicity (Fig. 1C, and fig. S1C). Cytotoxicity after exposure to 300 μM Mn was minimal in both GFP_Syn and GFP_EV cell groups, further confirming that αSyn protein

detected in the culture media resulted from the actual release of αSyn and was not due to cytotoxicity.

To further investigate the underlying molecular mechanisms of αSyn secretion and its relevance in the progression of neurodegenerative disorders, we further characterized the morphological features of the cargo behind αSyn secretion. Our analysis of differentially ultracentrifuged conditioned media through transmission electron microscopy (TEM) indicated the presence of nano-scale exosomal vesicles morphologically similar to previously reported exosomes (9) in both vehicle- and Mn-treated samples (Fig. 1D). Further analysis of cell lysates, conditioned media, and exosomes through Western blot analysis revealed that αSyn was primarily enriched in exosome fractions after Mn exposure (Fig. 1E). We also comprehensively assessed particle size and concentration in conjunction with protein analysis of purified exosomes to assess isolation efficacy and purity. Our Western blot analysis of isolated exosomes and whole cell lysates showed the presence of canonical exosome proteins, such as CD9, Alix, Flotillin-1, the diminished nuclear envelop marker Lamin, and the endoplasmic reticular protein GRP78, demonstrating a pure exosome preparation isolated using an ultrafiltration protocol (Fig. S1D). Furthermore, using the NanoSight LM10, we visualized, counted, and measured the size of exosomes isolated from GFP_Syn cells in the presence and absence of Mn. The average diameter of exosomes isolated from control cells was comparable to that of Mn-treated exosomes (150.8 ± 7.05 nm to 148.6 ± 12.42 nm, respectively; Fig. 1F), indicating that Mn exposure does not alter the size distribution of exosomes. These calculated sizes are consistent with previously published observations (6, 9).

We detected significantly more exosomes in the Mn-treated cells than in vehicle-treated cells (Fig. S1E), indicating that Mn exposure significantly enhances exosome release. The exosomal surface membrane protein markers Alix and Flotillin-1 were readily detected in all exosome samples (Fig. 1G). Notably, we observed more αSyn-GFP protein in the exosomes isolated from Mn-exposed cells than from untreated cells as determined by Western blot analysis (Fig. 1G), indicating that Mn increases the amount of αSyn in exosomal cargos. Similar results were obtained by quantitative ELISA analysis (Fig. S1F). To ensure that the enhanced exosome release was not driven by the GFP fluorescence tag, we explored the exosome release profile using a different protein tag based on a poly(His) affinity tag-bound αSyn protein. Naïve MN9D cells were transfected with either a 6X His-tagged human WT-αSyn-bearing plasmid or an empty 6X His plasmid. As described in previous experiments, cells were then treated with Mn and exosomes were isolated from conditioned medium. Using a dual color Western blot analysis, we readily detected the release of His-tagged αSyn as seen by co-localization of fluorescence secondary antibodies corresponding to 6X His (green) and human αSyn (red) (Fig. S1G). Furthermore, isolated exosomes exhibited the expected morphology (Fig. S1H), size profiles (Fig. S1I), and concentration (Fig. S1J), consistent with our observations of exosomes isolated from Mn-treated GFP_Syn cells.

The existence of αSyn oligomers in biological fluids and in exosomal fractions isolated from cultured cells (6, 11) has been well characterized. Therefore, using conformation-specific antibodies against prefibrillar oligomers (30) and specifically prefibrillar αSyn species (Fig. S1K), we sought to determine whether misfolded αSyn proteins accumulate in

exosomes of Mn-stimulated cells. When compared to exosomes isolated from vehicle-treated cells, accumulations of prefibrillar oligomers detected by A11 antibody noticeably increased in Mn-stimulated GFP_Syn exosomes, but not in Mn-stimulated GFP_EV exosomes (Fig. 1G, lower panel). Notably, our slot blot analysis using a newly developed αSyn antibody against filament readily detected an increased level of αSyn filament in Mn-stimulated exosomes isolated from GFP_Syn cells (Fig. 1G, lower panel), confirming that oligomeric protein accumulation resulted from Mn-induced αSyn protein misfolding. Furthermore, we measured misfolded αSyn oligomer abundance in these exosomes using the highly sensitive, Thioflavin T (ThT)-based αSyn fibril formation assay. In this microplate-based misfolded protein seeding assay, exosomes isolated from Mn- or vehicle-stimulated GFP_Syn and GFP_EV cells, serving as the seeds presumably with trace amounts of αSyn fibrils, are added to a recombinant human αSyn substrate and repeatedly agitated. By first optimizing the assay using different concentrations of synthetically aggregated αSyn as seed, we found that the onset of amyloid fibril formation, which increases fluorescence intensity when ThT binds to aggregates, directly correlated to αSyn fibril seed density (Fig. S1L). This correlation has previously been used to quantify the aggregation kinetics of two major forms of amyloid-β peptides and TSE-associated forms of prion protein (31, 32). Here, we found that Mn-stimulated GFP_Syn cell-derived exosomes (hereafter referred to as "αSyn exosomes") underwent nucleation-dependent seeded aggregation at a significantly higher rate than vehicle-stimulated αSyn exosomes (Fig. 1H). However, we didn't observe a marked increase in ThT readout in GFP_EV-derived exosomes (hereafter referred to as "GFP exosomes") treated with either Mn or vehicle (Fig. 1H). Collectively, our data suggest that Mn exposure increases the number of αSyn-containing exosomes released and upregulates the aggregated αSyn protein cargo packaged into these exosomes.

Mn-stimulated exosomes promote neuroinflammatory responses

Although exosomes play a major role in many physiological and pathological processes, the exosome-cell interaction mode and the intracellular trafficking pathway of exosomes in their recipient cells remain unclear. Feng and colleagues showed that exosomes are taken up more efficiently by phagocytic cells than by non-phagocytic cells, which suggests that phagocytic processes facilitate exosome uptake (33). This is particularly important in microglia, which are the resident macrophages in the CNS and whose phagocytic capabilities make them the first and primary active immune defense. Moreover, aberrant activation of glial cells and associated proinflammatory cytokines is increased in neurodegenerative diseases (3, 34, 35) and in experimental models of PD (36). Therefore, we exposed primary murine microglia to either vehicle- or Mn-stimulated exosomes to study whether Mn-stimulated exosomes have any role in neuroinflammatory processes.

We added purified exosomes to primary microglia and allowed their cellular internalization to occur for 24 hours at 37°C. Our immunocytochemical analysis with an anti-IBA and an anti-GFP antibody revealed GFP-positive punctate structures inside the microglia cells, indicating efficient exosomal internalization. However, only microglia exposed to Mn-stimulated αSyn-containing exosomes exhibited a pronounced amoeboid morphology resulting from the activation and formation of diverse surface protrusions, such as blebs and filopodia, similar to those of other phagocytic cells (Fig. 2A). The expression of IBA-1 and

iNOS, as revealed by Western blot analysis, increased significantly in cells treated with Mn-induced αSyn-containing exosomes in contrast to cells receiving vehicle-stimulated αSyn-containing exosomes, further confirming a distinct activation of microglia and subsequent inflammatory nitrative stress (Fig. 2, B to D). Supporting these observations, the release of proinflammatory cytokines, such as tumor necrosis factor α (TNFα), interleukin-12 (IL-12), IL-1β and IL-6, from microglia was significantly increased upon exposure to Mn-stimulated αSyn-containing exosomes, compared to vehicle-stimulated αSyn-containing exosomes or GFP control exosomes (Fig. 2E-H). These data collectively indicate that Mn-stimulated αSyn-containing exosomes are biologically active and capable of activating microglial cells and inducing the release of proinflammatory cytokines, which may further contribute to the inflammatory process.

Microglia internalize Mn-stimulated αSyn exosomes through caveolin-1–mediated endocytosis

The endocytic process in mammalian cells involves multiple mechanisms depending on the host cell type as well as cargo type and fate. So far, different modes of endocytosis seem to be responsible for the uptake of exosomes by both phagocytic and non-phagocytic cells (33, 37, 38). The previously described mechanisms of classical endocytosis include clathrin-dependent endocytosis, macropinocytosis and clathrin-independent endocytic pathways (such as caveolae-mediated uptake associated with lipid rafts in the plasma membrane). However, the mechanisms by which exosomes interact with recipient cells such as microglia and how exosomes are sorted after entry into these cells remain unclear. Therefore, we used a wild-type mouse microglial cell line (WTMC), that possesses morphology and surface marker expression that are highly similar to those of primary microglia (39), to determine which endocytic pathway microglia use to take up exosomes. As the initial pharmacological approach, we treated WTMC with various inhibitors of endocytosis, including dynasore, which binds dynamin to inhibit both caveolae- and clathrin-dependent endocytosis; (N-ethyl-N-isopropyl)-amiloride (EIPA), an inhibitor of macropinocytosis; and chlorpromazine and genistein, which inhibit clathrin- and caveolin-mediated endocytosis, respectively (37, 40).

To better visualize exosomal vesicles, the cell-derived exosomes were pre-labeled with the green fluorescent dye PKH67, which is stably incorporated into lipid regions of the vesicle membrane, and then incubated with WTMC cells. Confocal microscopy revealed efficient internalization of the vehicle- and Mn-stimulated αSyn-containing exosomes by the WTMC cell line (Fig. S2A). The 3D surface reconstruction images generated by Imaris software clearly revealed the homogeneous internalization of exosomes by the microglial cells and the activated microglial morphology upon internalization of Mn-stimulated, but not vehicle-stimulated, αSyn-containing exosomes (Fig. S2A). Next, we pre-treated WTMC with one of the endocytosis inhibitors, either chlorpromazine (5 μM), genistein (50 μM), EIPA (10 μM) or dynasore (50 μM), (40) for 60 min at 37°C. Subsequently, Mn-stimulated PKH67-labeled αSyn-containing exosomes were added and incubation was continued for 24 hours. Confocal microscopy (Fig. 3A) indicated successful inhibition (80–90%) of exosome uptake by dynasore and genistein, whereas EIPA and chlorpromazine were unable to effectively inhibit (50–60%) exosome uptake. Therefore, given its clathrin-independence and dynamin-

dependence during internalization, exosome uptake in our microglial cell cultures was primarily controlled through caveolae-dependent endocytosis. In a parallel experiment, we co-treated primary microglial cells with Mn-stimulated αSyn-containing exosomes and the endocytosis inhibitors to further analyze the production of proinflammatory cytokines and nitrite. Similarly, dynasore and genistein significantly attenuated the production of the proinflammatory cytokines TNFα, IL-1β and IL-6 in response to Mn-stimulated αSyn exosomes, whereas chlorpromazine and EIPA did so only marginally or not at all (Fig. 3, B to D). Dynasore, genistein and EIPA, but not chlorpromazine, significantly reduced nitrite production (Fig. 3E). Thus, these data indicate that the primary uptake of Mn-stimulated αSyn-containing exosomes by microglia involves caveolae-dependent endocytotic pathway.

Next, using primary murine microglial cultures, we confirmed the prominent role of caveolin-1-mediated endocytosis in microglial uptake of αSyn-containing exosomes. For this, we used fluorescently labeled transferrin and the cholera toxin B subunit (ctxB), which are widely recognized as ligands exclusively internalized via clathrin-mediated endocytosis and caveolae-mediated endocytosis, respectively, in several cell types (40, 41). Primary microglia cells were pre-treated with chlorpromazine or genistein as described above for 60 min at 37°C. At the end of the incubation, cells were co-treated for 24 hours at 37°C with one of either two combinations: Alexa-555-labeled transferrin and PKH67-labeled exosomes (Fig. S2B) or Alexa-555-labeled ctxB and PKH67-labeled exosomes (Fig. S2C). While chlorpromazine treatment significantly inhibited Alexa-555-conjugated transferrin uptake, it only moderately inhibited the uptake of PKH67-labeled exosomes or Alexa-555-conjugated ctxB (Fig. S2B). Cells treated with genistein exhibited 90–100% inhibition of both Alexa-555-conjugated ctxB and PKH67-labeled exosome uptake (Fig. S2C). Genistein, however, did not inhibit microglial uptake of transferrin. Therefore, our data suggest that caveolin-mediated endocytosis is the primary facilitator for the recognition and internalization of neuronal exosomes in a microglial cell model.

To further rule out the possible non-specific effects of pharmacological/chemical inhibitors, we next employed CRISPR/Cas9 nuclease RNA-guided genome editing to individually knockdown (KD) caveolin-1 or clathrin in the WTMC line to validate our experimental results involving chemical inhibition of endocytosis. The selective gene silencing of caveolin-1 and clathrin in WTMC was confirmed with Western blotting (Fig. S2D). In Luminex magnetic bead-based cytokine analysis, the release of the proinflammatory cytokines IL-6, IL-12, TNFα, and IL-1β was reduced significantly by exposing clathrin-KD cells to Mn-stimulated αSyn exosomes in contrast to control microglial cells (Fig. 3, F to I). A further reduction in αSyn exosome-stimulated proinflammatory cytokine release occurred in caveolin-1-KD cells. In contrast, we did not observed changes in anti-inflammatory cytokine IL-10 (Fig. S2E). Therefore, microglial internalization of exosomes derived from αSyn-expressing dopaminergic neuronal cells depends on multiple mechanisms, particularly the involvement of caveolin-1-dependent endocytosis.

Mn-stimulated αSyn exosomes induce neuronal cell death in vitro

After establishing the role of Mn-stimulated αSyn exosomes in activating neuroinflammatory processes in microglia, we expanded our experiments to evaluate

whether the exosomes play a role in neurodegeneration. For this purpose, we established a neuron-glia mixed culture system using primary microglial cells and differentiated human dopaminergic neuronal model referred to as LUHMES cells (Fig. S3A). Because LUHMES cells can be differentiated into morphologically and biochemically mature post-mitotic dopamine-like neurons, they are widely used as an *in vitro* model system for dopaminergic neurotoxicity (42). A Transwell® cell culture system enabled us to mimic their CNS environment by culturing pure microglial and neuronal cells separately but in close proximity within the same, shared culture media. Specifically, pure primary microglia were grown on porous upper inserts, while differentiated LUHMES cells were grown on a coverslip in the bottom well of the chamber (Fig. S3A). Thus, exposing the microglial cells to Mn-stimulated αSyn exosomes enabled us to observe significant Mn-stimulated αSyn exosome-mediated cytotoxicity or apoptosis, as indicated by increased caspase-3 activity in differentiated LUHMES cells (Fig. S3B). In contrast, GFP exosomes or vehicle-stimulated αSyn exosomes did not significantly increase caspase-3 activity, indicating that Mn-stimulated αSyn exosome-mediated cell death resulted from the combined effects of increased inflammation and oligomeric proteins packaged in Mn-stimulated αSyn exosomes. Exosome uptake readily occurred in exosome-treated LUHMES cells as evidenced by GFP-immunoreactive punctate structures inside the neuronal cells (Fig. S3C). Immunolabeling of the LUHMES cells with neuron-specific class II β-tubulin (Tuj1) confirmed the fully differentiated post-mitotic nature of the LUHMES cells, as described previously (42). Collectively, our data indicate that Mn-stimulated αSyn exosomes could initiate neuronal apoptosis through activation of neuroinflammatory processes in microglia.

Direct detection of Mn-induced cell-to-cell transmission of αSyn oligomers in vitro and in vivo

To further clarify the role of Mn in cell-to-cell transmission of αSyn aggregates, we adopted an assay based on bimolecular fluorescence complementation (BiFC), which has been successfully applied to assess protein oligomerization, protein-protein interaction and cell-to-cell transmission in *in vitro* and *in vivo* models (5, 6, 43). For this assay, human wild-type αSyn is fused to either the amino-terminal (V1S) or carboxy-terminal (SV2) fragment of the Venus protein, which is an improved variant of GFP (Fig. S4A). These two chimeras alone are not able to complement Venus fluorescence, which only occurs when the split Venus moieties fused with αSyn are brought together and covalently linked. V1S and SV2 constructs were individually transfected to MN9D cells, which were then co-cultured (Fig. 4A). Fluorescence resulting from dimerization or oligomerization of the V1S and SV2 fusion proteins (44) during cell-to-cell transfer of αSyn was visualized using BiFC (Fig. 4, A and B). The Mn-treated V1S/SV2 co-culture system exhibited a visually greater BiFC signal when compared to the vehicle-treated V1S/SV2 co-culture using confocal microscopy analysis (Fig. 4A), indicating that Mn stimulation indeed enhances cell-to-cell transmission of αSyn. To better understand the cargo mechanism of αSyn transmission, we used isolated exosomes found in conditioned medium collected from V1S and SV2 individually transfected cultures as well as V1S/SV2 co-culture systems. Western blot analysis of purified exosomes readily detected the αSyn immuno-positive V1S and SV2 protein fragments and the exosomal surface marker Alix in exosome lysates (Fig. 4C), implying exosomes as a possible cargo mechanism for cell-to-cell transmission of αSyn. Furthermore,

when V1S and SV2 BiFC constructs were individually transfected into MN9D cells, neither cells fluoresced (Fig. 4B, left two panels). However, once cells were co-transfected with V1S and SV2 (right two panels), αSyn-αSyn interactions (6) reconstituted the Venus fluorescent protein (Fig. 4B). Moreover, the formation of reconstituted Venus fluorescent protein sharply increased in Mn-treated co-transfected cells (Fig. 4B, right two panels), confirming that Mn exposure enhances αSyn aggregation.

To study the nature of αSyn species visualized by the BiFC assay, total cell lysates were separated with Western blotting and immunoblotted with an anti-ubiquitin antibody. As expected, cells co-transfected with V1S and SV2 followed by Mn treatment accumulated both as high-molecular-weight poly-ubiquitinated proteins, indicating that Mn enhanced protein oligomerization when compared with vehicle-treated cells (Fig. S4B). Using αSyn and GFP antibodies, we also detected discrete bands corresponding to Venus-link-αSyn (V1S) and αSyn-Venus (SV2) protein expression and their N-terminal Venus fluorescent tag (Fig. S4B).

To ensure αSyn oligomerization and transmission were not driven by the Venus fluorescent moieties, we adopted another protein complementation assay based on a luciferase assay system consisting of the two fusion constructs αSyn-hGLuc1 (S1) and αSyn-hGLuc2 (S2) as described elsewhere (6, 44). While this assay utilizes the same principle as the BiFC assay, *Gaussia princeps* luciferase only reconstitutes with S1 and S2 protein interaction, allowing direct monitoring of αSyn-αSyn protein interactions in their normal cellular environment. Co-transfection of S1 and S2 constructs showed about 5-fold higher luciferase activity relative to the background signal from cells transfected with either S1 or S2 plasmids alone. Furthermore, exposure of S1 and S2 co-transfected cells to Mn significantly increased luciferase activity relative to vehicle-treated S1+S2 co-transfected cells (Fig. S4C). These data are consistent with our fluorescent-based BiFC assay results and support our finding that Mn exposure induces misfolded αSyn species.

Finally, cells co-transfected with V1S and SV2 and treated with either Mn or vehicle for 24 hours were fixed and processed for flow cytometry analysis to further confirm that Mn promotes cell-to-cell transmission of oligomeric αSyn. Since the reconstituted Venus fluorescent protein formed in the BiFC experiment matures at 37°C as a strong fluorescent signal, we used fluorescence-activated cell sorting (FACS) to contrast GFP-positive cell populations exposed to Mn or vehicle treatments (Fig. 4D). Our FACS analysis shows significantly more GFP-positive cells in Mn-exposed cells than in the vehicle-treated control group (Fig. 4E). Consistent with our BiFC assay, we did not detect GFP-positive cells when transfected with either V1S or SV2. Thus, using multiple experimental approaches, we demonstrate that Mn exposure promotes cell-to-cell transmission of αSyn in our cell culture system.

Once we established the effect of Mn on cell-to-cell transmission of oligomeric αSyn cell culture models, we attempted to further confirm our findings using animal models of Mn toxicity. We used an *in vivo* protein complementation approach consisting of co-injecting AAVs encoding αSyn fused to the N- or C-terminal half of Venus fluorescent protein (43). Thirty days after stereotaxically co-injecting AAV8-V1S and AAV8-SV2 into the SNpc of

C57BL/6 mice (Fig. S4D), animals were exposed to either vehicle or Mn (15 mg/kg/day) via oral gavage once daily for another 30 days (Fig. S4D). Two additional control groups were injected with either AAV8-V1S or AAV8-SV2 virus to exclude the possibility of non-specific fluorescence from one-half of the VenusYFP protein, and another group was injected with AAV8-CBA-VenusYFP as a positive control for the experiment. At 60 days post-viral injection, the VenusYFP fluorescence that had colocalized in TH-positive cells was clearly visible in the SNpc of animals injected with AAV8-CBA-VenusYFP, confirming our injection target and the expression of VenusYFP epifluorescence (Fig. 4F).

To determine whether Mn exposure promotes αSyn oligomerization and pathogenesis *in vivo*, we used the Kodak In-Vivo FX Image Station to study VenusYFP expression and localization in vehicle-treated and Mn-exposed mice. Using MATLAB, we captured and converted whole brain fluorescent images into heat-maps, which were then superimposed on white-light reference images to show anatomical localization of VenusYFP fluorescence (Fig. 4G). Quantification of fluorescent intensities clearly indicates that Mn promoted V1S and SV2 protein–protein interactions resulting in αSyn oligomerization, which increased about 350% in Mn-exposed animals when compared to vehicle-treated animals (Fig. 4H). Notably, control animals injected with either AAV8-V1S or AAV8-SV2 alone did not express any VenusYFP fluorescence on the injected side, demonstrating that the fragmented Venus protein lacks background fluorescence.

Because our *in vivo* study of αSyn-mediated neurotoxicity targeted the SNpc, we also assessed the locomotor behavioral performance of V1S- and SV2-co-transduced and non-transduced mice exposed to Mn via oral gavage. Non-transduced and transduced mice were age-matched littermates and the Mn or vehicle exposures were conducted simultaneously. After the 30-day Mn treatment paradigm, we measured locomotor performance using a computerized infrared activity monitoring system (VersaMax, Accuscan), which quantifies animal movement variables based on infrared beam breaks. Representative maps of the locomotor movements of vehicle-treated and Mn-treated non-transduced (no injection) and transduced (AAV8-V1S+AAV8-SV2) mice suggest that Mn decreased movements in both experimental groups and that viral-transduced mice exhibited greater Mn-induced movement deficits (Fig. 4I). Mn markedly decreased the total number of movements (Fig. 4J), total distance travelled (Fig. 4K), and horizontal activity (Fig. 4L) in transduced mice compared to vehicle-treated animals. Our results suggest that αSyn misfolding mediates neurotoxicity and impairs locomotor behavior and that Mn exposure augments behavioral deficits.

Next, we examined nigral dopaminergic neuronal viability after a 30-day Mn exposure period in both AAV8-V1S+AAV8-SV2 co-transduced and non-transduced animals. Coronal sections through the SN were immunostained for tyrosine hydroxylase (TH) and visualized by diaminobenzidine (DAB) (Fig. 4M). Dopaminergic neuronal loss was evaluated using unbiased stereology of TH-immunoreactive neurons on both the ipsilateral and contralateral sides. DAB staining and stereological counting of TH^+ neurons revealed severe loss of nigral dopaminergic neurons, especially in the SNpc and SNpl of Mn-treated AAV8-V1S+AAV8-SV2 co-transduced animals relative to vehicle controls (Fig. 4N). These observations show that Mn-induced cell-to-cell transmission of oligomeric αSyn promotes nigral dopaminergic neurodegeneration *in vivo*. In contrast, Mn-exposed non-transduced animals showed no

significant loss of TH^+ neurons when compared to their vehicle control animals. Overall these results, together with the abovementioned whole brain imaging of the cell-to-cell transmission of αSyn, strongly demonstrate that exposure to the environmental neurotoxicant Mn can augment the progression of cell-to-cell transmission of oligomeric αSyn *in vivo,* resulting in dopaminergic neuronal degeneration.

Mn exposure promotes exosome release in αSyn-A53T transgenic animals and correlates with αSyn oligomer transmission in humans

Having shown that exposing virally transduced mice to Mn induces cell-to-cell transmission of oligomeric αSyn and dopaminergic neurodegeneration, we then evaluated the effect of Mn exposure on serum exosome release in αSyn transgenic and littermate control rats. In this study, we used a newly developed BAC (bacterial artificial chromosome) transgenic rat model of PD expressing the A53T mutation of αSyn, which is known to cause early-onset autosomal dominant PD in humans. The mutant human αSyn transgene protein was expressed at an amount ~42-fold above that of endogenous αSyn in transgenic rats (45). The A53T mutation was not detectable in wild-type Sprague Dawley control rats. Both non-transgenic and transgenic rats were treated with Mn as described above and their blood was collected through cardiac puncture at study termination. Serum separation and exosome isolation were carried out as described and total serum exosome numbers were counted using the NanoSight particle analyzer. Mn-challenged αSyn-A53T transgenic rats produced significantly higher concentrations of exosomes than did either vehicle-treated transgenic rats ($P = 0.0035$) or non-transgenic rats ($P = 0.0082$) (Fig. 5A). Furthermore, Mn exposure did not alter exosome size, but only increased the number of exosomes released (Fig. 5B). Therefore, exosomes may act not only as a means of cell-to-cell communication during increased intracellular stress conditions, but also as a cargo mechanism for secretion and cell-to-cell transmission of harmful or unwanted cellular proteins.

It has been proposed that exogenously added misfolded αSyn serves as nucleation seeds for propagating aggregate-initiated polymerization of αSyn in in vitro and in vivo models of PD (15–17, 46). Since exosomes are well recognized as one of the potential mechanisms mediating cell-to-cell transmission of cytosolic protein aggregates (47), and given the strong interaction between metal exposure and PD (24, 48–50), we undertook an exploratory study of the effects of Mn exposure on αSyn transmission in humans. As a group, welders are at risk of prolonged exposures to environmental levels of metals, including Mn, that can be neurotoxic (21, 29, 51). We compared the exosomal αSyn content in serum from welders exposed to Mn fumes (aged 26–65 years, mean 46 ± 11.2 years; n = 8 individuals; serum obtained within 90 days of the study) to that found in serum from healthy controls (aged 28–73 years, mean 49 ± 11.0 years; n = 10 individuals) with no history of welding [see details in Lee *et. al* 2015 (22) for the first description of the subjects, as well as Lee 2016 (23)]. Serum exosomes were isolated as described above and total αSyn concentrations in these exosomes were analyzed using a commercially available, highly sensitive luciferase-based αSyn ELISA kit. Total αSyn cargo in the serum exosomes did not differ ($P = 0.2855$) between welders and controls (Fig. 5C). We also counted total exosome numbers using NanoSight particle analysis. Contrary to our previous observations with transgenic cells and rats, the exosome counts of welders did not differ significantly from that of controls (Fig. 5D). One

possible explanation accounting for this result is that the extent of Mn exposure experienced by these welders was not sufficient to alter their serum exosome numbers or total αSyn cargo.

Though the outcome we observed in humans did not directly support changes observed in transgenic cells and rats, widely varying αSyn abundance in peripheral blood and CSF samples has been reported in PD patients relative to healthy controls (2, 52, 53). Notably, in the αSyn model of neuron injury, β-sheet-rich soluble oligomers are considered more toxic than monomers (54, 55). Therefore, we measured the abundance of αSyn oligomers in these human exosomes using the αSyn fibril formation assay. Blank and baseline-corrected average kinetic traces for seeded αSyn fibrillar formation assays revealed a significantly different lag-phase between the averaged traces of welder exosome samples and those of control individuals. The lag-phase duration was determined from the point where the ThT fluorescence intensity first reached the amyloid detection threshold (Fig. 5E), defined as five standard deviations of the fluorescence intensity of the first 10 hours for the blank (3.66) sample. Standard error of the mean lag-phase was calculated via bootstrap with replacement protocol in MATLAB. The calculated lag-phases for control and welder exosomes were 75.5 hours and 42.5 hours, respectively. Furthermore, we calculated final fluorescence intensity to compare two kinetic traces by averaging the raw ThT fluorescence of the last 10 data points of each trace (Fig. 5F). Mean ThT fluorescence intensities for controls and welders differed significantly ($P < 0.001$), indicating that exosomes isolated from welders have a higher seeding capacity and misfolded αSyn protein content compared to exosomes isolated from healthy controls. This exciting observation further validated with dot blot analysis with antibody against fibrillary αSyn (Fig. 5, G and H). Together, our data indicate that environmental exposure to neurotoxic metals, such as Mn, increases the abundance of misfolded protein cargo in circulating exosomes. However, given the limitations associated with sample isolation and collection, it must be noted that blood-derived exosomes are an indirect measure of cell-to-cell transmission in the CNS. As such, it is unclear whether the results shown here are due to exosome clearance from the blood or are exosomes released by affected neurons into the systemic circulation. Nevertheless, previous reports indicate the presence of CNS-derived αSyn in plasma exosomes in PD patients (56) and increased phosphorylated tau and beta amyloid (Aβ) proteins in blood-derived exosomes in Alzheimer's disease patients (57), further suggesting a role of exosomes in disease pathogenesis.

Mn-stimulated αSyn exosomes induce Parkinson-like motor deficits in mice

The accumulation of misfolded proteins and associated behavioral deficits are fundamental pathogenic processes in the progression of PD (46). Furthermore, evidence from recent in vitro and in vivo studies suggests that misfolded proteins play a central role in a variety of neurodegenerative disorders by functioning as "seeds" for progressive protein misfolding and aggregation processes, much like prions (58, 59). Thus far, we have shown that Mn-stimulated exosomes contain prefibrillar αSyn oligomers that potentiate neuroinflammatory and degenerative responses in vitro. As a next step, we directly investigated whether Mn-stimulated αSyn exosomes carry disease-associated prefibrillar αSyn oligomers, which can seed and propagate pathology in vivo. We injected C57BL/6 mice with exosomes isolated

from Mn- or vehicle-treated GFP_EV and GFP_Syn cells. Approximately, 4–5 × 10^8 exosomal particles (~8 μg total exosome proteins) from each treatment group were stereotaxically injected into one side of the striatum (Fig. 6A) and neurobehavioral deficits were monitored over time. The behavioral performance of animals injected with αSyn exosomes tended to worsen when tested again at 180 days post-inoculation (dpi). Specifically, mice receiving Mn-stimulated αSyn exosomes tended to be more hypoactive, showing reduced exploratory locomotor activity as measured by stereotypy counts (Fig. 6B) in an open field locomotor test. However, some behavioral deficits, such as movement time (Fig. 6C), were not statistically significant, perhaps because exosome injections were done unilaterally and the observed αSyn-containing proteinaceous inclusions were primarily localized in cortical-striatal regions proximal to the injection site. PD has long been recognized as an asymmetric disorder, with unilateral motor symptom onset as one of its cardinal features, especially in patients classified as early-stage PD (60–62). The etiology of these asymmetric motor symptoms remains unclear, although several hypotheses involving lateralized vulnerability, an index of abnormal protein deposition, have been advanced (60, 61). To test for a possible behavioral bias arising from exosome-induced behavioral asymmetry, we used the amphetamine-induced rotation test. Interestingly, our data indicate increased ipsilateral movements in the Mn-stimulated αSyn exosome-injected mice, thus indicating unilateral CNS damage in these animals, when compared to mice receiving vehicle-stimulated αSyn exosomes or vehicle- and Mn-stimulated GFP exosomes (Fig. 6D). Although the mechanism for the unilateral behavioral bias encountered here is not completely understood, it likely involves an increase in neurodegenerative processes induced by ipsilaterally localized, αSyn-containing proteinaceous inclusions.

To confirm in vivo αSyn misfolding, we examined whether Mn-stimulated αSyn exosomes lead to the deposition of αSyn-containing proteinaceous inclusions. Histological analyses revealed Ser^{129}-phosphorylated αSyn (pSyn129) and p62-immunoreactive cytoplasmic inclusions in mice injected with Mn-stimulated αSyn exosomes (Fig. 6E), but not in mice injected with vehicle-stimulated αSyn exosomes or vehicle- and Mn-stimulated GFP exosomes (fig. S5, A to F). Furthermore, our dual-staining with pSyn129 and microglia marker IBA-1 indicate the microglial cells with larger cell body and shorter processes around the pSyn129 positive neurons, indicating Mn-stimulated αSyn exosomes trigged inflammatory response in brain. In contrast, animals injected with vehicle-stimulated αSyn exosomes resulted in no pSyn129 pathology in cortical regions (Fig. S5A) and minimal pathology around the striatal injection site (Fig. S5D). Mice receiving vehicle-stimulated GFP exosomes (Fig. S5, B and E) or Mn-stimulated GFP exosomes (Fig. S5, C and F) did not exhibit any protein inclusions or GFP immuno-positive structures, suggesting that the GFP protein may have been cleaved-off and degraded. Collectively, our results clearly indicate that Mn-stimulated, αSyn-containing exosomes can initiate certain Parkinsonian symptoms and propagate αSyn misfolding and aggregation in mice. Collectively, our experimental results have important implications pertaining the prion-like, cell-to-cell transmission of aggregated proteins in progressive neurodegenerative disorders.

Discussion

Chronic occupational exposure to metals, especially to Mn through welding, mining, and smelting, has been reported as a putative risk factor for environmentally-linked Parkinsonism and related neurodegenerative disorders (21, 24, 48). Chronic exposure to low dose Mn through food, water and air has been linked to neurological impairment (66). Though previous studies link Mn neurotoxicity to neuronal apoptosis and αSyn upregulation and aggregation in experimental models of Parkinsonism (3, 28, 65), its role in the release and transmission of pathogenic αSyn has not been studied. Therefore, to further understand the role of Mn in the cellular release of αSyn, we systematically carried out experiments to show that Mn increases the release of misfolded αSyn-containing exosomes, which could increase neuroinflammatory and neurodegenerative responses in experimental models of Parkinsonism.

Our WT human αSyn-expressing cell culture model clearly demonstrates that Mn enhances the release of extracellular αSyn, providing direct *in vitro* evidence linking exposure to neurotoxic metals and αSyn release. Since αSyn lacks a signal recognition sequence required for the conventional ER/Golgi secretion pathway (67), several unconventional secretion mechanisms have been implicated in αSyn release, including an endosomal pathway that directs the transfer across the membrane for exosomal release (9, 11). Therefore, to characterize the mode of αSyn release induced by Mn, we analyzed conditioned media through TEM and Western blotting. We readily detected micro-vesicles similar in size, morphology and expressing proteins such as Alix and Flotillin-1 that are common to these exosomes. Particularly, αSyn-expressing cells exposed to Mn released substantially more αSyn oligomer-containing exosomes, thus providing compelling evidence of the role of environmental neurotoxicants in exosome biology.

Extracellular αSyn reportedly interacts with CD36 (10), toll-like receptor 4 (TLR4) (70) and TLR2 (63), and thus activates microglial inflammatory processes and enhances ROS production. Using WT microglial cells and a LUHMES-primary microglia co-culture model, we demonstrate that Mn-stimulated αSyn exosomes were taken up by microglia through caveolae-mediated endocytosis, eliciting the release of pro-inflammatory cytokines. It is probable that the inflammatory milieu and presence of oligomeric/amyloid αSyn in this co-culture medium led to up-regulation ofcaspase-3 in differentiated LUHMES cells, demonstrating that misfolded αSyn-containing exosomes contribute to neuronal cell death by activating the neuroinflammatory response. These results support recent observations indicating that neuroinflammation plays a major role in PD (36).

Our study also provides direct evidence that Mn exposure enhances αSyn transmission. We show that Mn treatment leads to more BiFC-positive cells and greatly increased extracellular V1S/SV2 exosomal protein content, demonstrating for the first time that Mn not only causes αSyn oligomerization but also stimulates its cell-to-cell transmission. We confirmed these *in vitro* findings in animals, showing a much elevated BiFC-positive signal in animals exposed to Mn, further supporting the notion that overexposure to neurotoxicants triggers αSyn misfolding and increase its cell-to-cell transmission. Previously, we showed that physiological levels of human WT αSyn attenuate acute Mn-induced dopaminergic neuronal

degeneration in cell culture models, but that prolonged Mn exposure promotes αSyn aggregation and neurotoxicity (71). Several studies show that Mn accumulation in the globus pallidus and associated striatal brain structures leads to GABAergic and dopaminergic neurotoxicity (72–74), but few have addressed Mn's long-term effects in animal models or in humans. Findings from neuroimaging and neurobehavioral studies of humans exposed to Mn through mining or welding are inconclusive due to conflicting outcomes on the possibility of nigrostriatal dopaminergic neuronal degeneration (24, 48, 49, 51). In fact, Mn can decrease dopamine turnover in the striatum of transgenic mice expressing human wild-type αSyn without inducing nigrostriatal degeneration (75). Despite the discrepancies in the published literature on Mn-induced dopaminergic neurodegeneration, we clearly observed Mn-induced TH^+ neuron loss and related behavior deficits in animals transduced with V1S/SV2 AAV8. This may result from Mn-induced αSyn oligomerization *in vivo,* which ultimately harms dopaminergic cells. Therefore, these findings have important implications for our current understanding of gene-environment interactions in PD.

Another important finding of this study is that Mn also markedly elevated concentrations of serum exosomes in A53T-αSyn transgenic rats, suggesting a strong correlation between the effects of genetic risk factors and environmental neurotoxicants on exosome release. Although we did not see higher exosome numbers or more αSyn in exosomes isolated from humans exposed to Mn-containing welding fumes, our study of active, asymptomatic welders was constrained by our inability to measure actual brain Mn levels and to obtain serum samples under controlled conditions from a more precisely defined population of known exposure levels. Nevertheless, we report that these welders do contain higher misfolded αSyn content in their serum exosomes, which may explain previous epidemiological studies identifying welding as a putative risk factor for developing PD-related neurological symptoms in later life (21, 24, 49). A recent longitudinal study on αSyn in blood plasma detected enhanced Ser129-phosphorylated αSyn despite no changes in "total αSyn" levels (76). Given that Ser129-phosphorylated αSyn has been positively identified in approximately 90% of Lewy bodies (77), the presence of αSyn in body fluids points to a promising early biomarker for PD. These extracellular forms of αSyn could play an important role in the prion-like, cell-to-cell transmission of αSyn pathology in the brain since αSyn can cross the BBB and spread throughout the CNS, resulting in distinct synucleinopathies after administration of misfolded αSyn through intravenous (78), intramuscular (79) or gastric injection (80). Given that exosomes are natural nano-scale transport vesicles capable of readily delivering siRNA and biologically active molecules *in vivo* across the blood-brain barrier (81), the detection of aggregated αSyn-rich exosome cargo in welders exposed to Mn strengthens the potential implications of our findings. However, since these welder cohorts likely present multiple etiologies, and possible exposure to multiple metals and confounding variables (such as disease states, ergonomics, other exposures, and age), demonstrating clinical significance remains problematic. Still, misfolded αSyn in serum exosomes should be studied more systematically as a noninvasive diagnostic biomarker for familial and sporadic PD.

We also evaluated whether exosomes function as a "seed" for the protein misfolding and aggregation process in experimental models of PD. Having shown that Mn induces αSyn-expressing cells to produce exosomes rich in αSyn oligomers, our unilaterally injecting

αSyn oligomer-bearing exosomes into the mouse striatum produced nucleation-dependent protein misfolding effects, as revealed by strongly ipsilaterally biased rotation test results, only in the group injected with Mn-stimulated αSyn exosomes. We also detected p62 and Ser129-phosphorylated αSyn-immuno-positive inclusion bodies, indicating that exosomal αSyn propagates *in vivo*, resulting in inclusions resembling Lewy bodies and Lewy neurites, as reported elsewhere (16, 46, 59).

In conclusion, we identified a possible mechanism involving the exosome-mediated, cell-to-cell transmission of αSyn during exposure to the environmental neurotoxicant Mn. Importantly, we show in animal models of metal-induced Parkinsonism that Mn exposure upregulates the release of αSyn-packed exosomes capable of propagating and inducing neurotoxicity. We also report elevated levels of oligomeric αSyn in the circulating exosomes of humans exposed to Mn through welding fumes, providing human translational relevance to our experimental results. More well-designed epidemiology studies are needed that combine detailed histories of occupational Mn exposure with both behavioral and other endpoints of Mn neurotoxicity. The significance of our findings might be relevant to other environmental toxicants implicated in protein-misfolding diseases and possibly to the development of interventional strategies to dampen exosome-mediated disease progression.

Materials and Methods

Chemicals and Reagents

Advanced DMEM/F-12, DMEM/F-12, Neurobasal medium N2 supplement, B27 supplement, fetal bovine serum (FBS), L-glutamine, Lipofectamine 2000, Alexa fluorophore-tagged secondary antibodies, Hoechst nuclear stain, penicillin, streptomycin, and other cell culture reagents were purchased from Life Technologies (Gaithersburg, MD). Antibodies for rabbit iNOS and Syn 211 were purchased from Santa Cruz Biotechnology, Inc. (Santa Cruz, CA). Mouse tyrosine hydroxylase (TH) antibody, Alix, A11, IBA-1, GFP and fibrillar confirmation-specific αSyn antibodies were purchased from Millipore (Temecula, CA). Antibodies for LDHA, clathrin and caveolin-1 were obtained from Cell Signaling (Danvers, MA). Antibody for phosphorylated (S129) αSyn and IBA-1 (rabbit) were purchased from Wako. Ubiquitin antibody was purchased from Dako (Carpinteria, CA). Mouse β-actin antibody, PKH67 and all other chemicals were obtained from Sigma (St. Louis, MO). Western blot supplies and the Bradford protein assay kit were purchased from Bio-Rad Laboratories (Hercules, CA). To construct the GFP-fused αSyn plasmid (αSyn-pMAXGFP), human wild-type αSyn cDNA was subcloned to pmaxFP-Green-N (Lonza) from the α-SYN-pCEP4 (71) plasmid. The mammalian expression plasmid for the N-terminal hemagglutinin (HA)-tagged and C-terminal-His'-tagged wild-type human αSyn (pHM6-alphasynuclein-WT) was a kind gift from Dr. David Rubinsztein (Cambridge; Addgene plasmid # 40824) (88). The bacterial expression plasmid bearing the wild-type human αSyn (pT7–7 αSyn WT) was a kind gift from Dr. Hilal Lashuel (Swiss Federal Institute of Technology-Lausanne; Addgene plasmid # 3604) (89). The αSyn BiFC plasmids, Gaussia luciferase protein fragment complementation assay plasmids [αSyn-hGLuc(1) and αSyn-hGLuc(2)], pAAV8-CBA-Venus1-Synuclein-WPRE (AAV8_V1S), pAAV8-CBA-Synuclein-Venus2-WPRE (AAV8_SV2) and pAAV8-CBA-Venus

(AAV8_venusYFP) virus were kindly provided by Dr. Pamela J. McLean (Mayo Clinic, Jacksonville, FL) and generated as described previously (43, 44). Recombinant αSyn monomers and fibrils were gifts from the Michael J. Fox Foundation for Parkinson's Research.

Cell cultures and stable expression of αSyn

For αSyn release and exosome isolation experiments, we created a GFP-tagged αSyn stably-expressing MN9D dopaminergic cell line. Expression plasmids encoding human full-length αSyn-pMAXGFP and control pMAXGFP (Lonza) were transfected into MN9D cells using Lipofectamine 2000 reagent and grown in DMEM (D5648; Sigma) supplemented with 50 IU/ml penicillin, 50 μg/ml streptomycin, and 10% FBS. For stable transfection, MN9D cells were selected after culturing in 400 μg/ml of geneticin for one week after transfection and then maintained in media supplemented with 200 μg/ml of geneticin. GFP-positive αSyn-expressing (GFP_Syn) and vector control (GFP_EV) cells were further selected by the FACSAria III (BD Bioscience) high-speed sorting flow cytometer to obtain homogeneously transgene-expressing cell populations.

Primary murine microglial cells were isolated from mixed cultures prepared from C57BL/6 mouse pups, postnatal days P0 to P1, using a column-free magnetic separation method as previously described (90). Exosome-induced neurodegeneration experiments were carried out with primary mesencephalic cultures and differentiated Lund human mesencephalic (LUHMES) cells. Primary mesencephalic neuronal cultures and LUHMES cells were grown and differentiated as previously described (91–93).

The immortalized wild-type (C57BL/6) murine microglial cell (WTMC) line, with morphology and surface marker expression highly similar to primary murine microglia, was a kind gift from Dr. Douglas Golenbock at the University of Massachusetts Medical School, Worcester, MA (39). These cells were grown in DMEM medium supplemented with 50 IU/ml penicillin, 50 μg/ml streptomycin, and 10% FBS, with exosome stimulation done in 2% DMEM. The WTMC was used for exosome-induced neuroinflammation experiments and identification of a possible endocytic pathway. Knockdown of caveolin-1 and clathrin was achieved using the CRISPR/Cas9 nuclease RNA-guided genome editing system in primary microglia cells. The lentivirus-based CRISPR/Cas9 plasmids, pLV-U6g-EPCG-Cav1 and pLV-U6g-EPCG-Cltc with the caveolin-1 and clathrin gRNA target sequences GTTGAGATGCTTGGGGTCGCGG and TACTGAAGCCAATGTTTGCTGG, respectively, were purchased from Sigma-Aldrich. To make lentivirus, the lenti-CRISPR/Cas9 Cav1 and C1tc plasmids and control plasmid were transfected into 293FT cells using the Mission Lentiviral Packaging Mix from Sigma-Aldrich, according to manufacturer's instructions. The lentivirus was harvested over 72 hours post-transfection and added to the microglial cell line to knockdown Caveolin-1 and Clathrin expression.

Media protein precipitation for Western blot

Following treatment, 2 ml of media was collected, and exosomes were isolated using ExoQuick TC. Following exosomes isolation, media was transferred into fresh tubes. An equal amount of methanol was added to the media. Following methanol addition, 200 μl of

chloroform was added to the mixture and mixed vigorously for 30 sec. The samples were spun down at 13000 × g for 5 min at 4°C. After three phases appeared, the aqueous part was removed, and protein was kept. The protein was vortexed until white flakes appear. We centrifuged at 15000 × g for 5 min at 4°C and removed the supernatant following centrifugation. Tubes were dried at 55°C in a thermoshaker at 300 × g for 5–10 min. Pellets were reconstituted in 40 μl of 1× Dye.

Immunocytochemistry and Immunohistochemistry

For immunocytochemistry, MN9D cells and microglia cells were plated on 50 μg/ml poly-D-lysine-coated 12-mm glass coverslips and treatments were done as described. LUHMES cells were plated on coverslips pre-coated with 50 μg/ml poly-l-ornithine (Sigma-Aldrich) overnight, washed twice with cell culture grade water (Invitrogen) and then incubated with 1 μg/ml fibronectin (Sigma-Aldrich) overnight. After treatments, cells were washed with PBS and incubated in 4% paraformaldehyde for 30 min at RT. After fixing, the cells were washed with PBS and incubated in blocking agent (2% BSA, 0.05% Tween-20, and 0.5% Triton X-100 in PBS) for 45 min. Cells then were incubated with antibodies against human αSyn (Syn 211; Santa Cruz, 1:500), GFP (Abcam 1:2000), and IBA-1 (Wako, 1:500) overnight at 4°C or the cytoskeleton marker Phalloidin (Alexa Fluor 647 phalloidin, Invitrogen) for 30 min at RT. After primary incubation, the cells were washed and incubated in the dark for 90 min with Alexa-488 and −555 dye-conjugated secondary antibodies (Invitrogen, 1:1000). Hoechst 44432 was used as a nuclear stain and the coverslips were then mounted on glass slides and viewed with 63× and 43× oil objectives using a Leica DMIRE2 confocal microscope. Photomicrographs were further processed using Imaris software to analyze the Z-stack images for exosome internalization. Using 3D surface reconstruction, we generated surface topology images using the maximum intensity projection (MIP) image.

For immunohistochemistry studies, fixed brains embedded in optimal cutting temperature (OCT) compound were sectioned at 30 μm using a cryostat (CryoStar NX70, Thermo Scientific) or processed as 7-μm paraffin-embedded sections. Free-floating sections were processed for immunohistochemical analysis as described in our previous publications (94, 95) using antibodies against TH (clone LNC1; Millipore, 1:1200). Diaminobenzidine (DAB) immunostaining was performed on substantia nigra sections as described previously (94–96) for stereological counting of TH^+ neurons. Briefly, 30-μm sections were incubated with anti-TH antibody overnight at 4°C. Then, sections were incubated with biotinylated anti-rabbit secondary antibody (1:300, Vector Labs) for 1 hour at RT followed by incubation with avidin peroxidase (Vectastain ABC Elite kit, Burlingame, CA). Immunolabeling was visualized by exposure to 0.5 mg/ml DAB, 2.5 mg/ml nickel ammonium sulfate and 0.03% H_2O_2 followed by incubation with hematoxylin nuclear counterstain (Vector Hematoxylin QS, H-3404). Sections were mounted on charged glass slides, dehydrated to xylene and coverslipped with DPX mounting medium (Sigma, Cat# 44581). Total numbers of TH-stained neurons in the SN were counted stereologically with Stereo Investigator software (MicroBrightField, Inc., Williston, VT) using an optical fractionator. For pS129 αSyn studies, 7-μm thick paraffin-embedded sections of mouse tissues were deparaffinized and subjected to overnight antigen retrieval using citrate buffer. Sections were then incubated with blocking reagent (10% normal goat serum, 2% BSA, and 0.5% Triton X-100 in PBS)

for 60 min before being incubated with a mouse monoclonal antibody against Ser^{129}-phosphorylated human αSyn (pSyn129/81A 1:5000). Immunolabeling was visualized with DAB peroxidase (with Nickel) or Vector SG (Vector Laboratories) substrate kits.

Western and Slot blotting

Whole cell lysates or exosome lysates were prepared using modified RIPA buffer containing protease and phosphatase inhibitor cocktail (Thermo Scientific, Waltham, MA), as described previously (71, 97). For αSyn release experiments, GFP_Syn and GFP_EV cells were treated in serum-free medium and spiked with 10 μg/ml BSA, and then the media was collected and centrifuged for 5 min at 3000 × g to remove any dislodged cells or cell debris. The conditioned media was concentrated using 5000 MWCO Vivaspin-20 spin columns (GE Life Sciences), and then protein concentrations were determined with the Bradford protein assay kit. Cell lysates containing equal amounts of protein were separated on a 12–15% SDS-polyacrylamide gel. After separation, proteins were electro-blotted onto a nitrocellulose membrane and nonspecific binding sites were blocked by treating with LI-COR blocking buffer. Primary antibodies for Syn-1 (BD Bioscience), Flotillin-1 (BD Bioscience), BSA (Invitrogen), LDHA (Cell Signaling), Aip1/Alix (Millipore), IBA-1 (Wako), iNOS (Santa Cruz), and β-actin (Sigma) were used to blot the membranes.

The formation of oligomeric proteins following Mn exposure was analyzed with a slot blot apparatus (Bio-Dot, Bio-Rad) using the antibody against protein oligomers (A11, Invitrogen) and αSyn filament specific antibody (MJFR-14–6-4–2, Abcam). Following protein adsorption, membranes were blocked with 5% BSA and incubated overnight with the A11 antibody or αSyn filament antibody. Membranes then were developed with IR800-conjugated anti-rabbit or Alexa Fluor 680-conjugated anti-mouse secondary antibody for 1 hour at RT. Western and slot blot (SS) images were captured with the Odyssey IR Imaging system (LI-COR) and data were analyzed using Odyssey 2.0 software.

Exosome isolation

Cell-produced exosomes were isolated using the ExoQuickTC (System Biosciences) exosome precipitation reagent or were purified by differential ultracentrifugation via slight modification of a process described previously (9, 12). Briefly, GFP_Syn and GFP_EV cells at 70–80% confluency were treated with or without 300 μM Mn in exosome-depleted medium containing 10% FBS for 24 h. After treatment, cell culture supernatant was collected and spun at 300 × g for 10 min to remove cells and 10,000 × g for 15 min to exclude cell debris from the supernatant. The resulting media then was passed through a 0.2-μm syringe filter (Millipore) to remove any remaining particles or cell debris, and the filtrate was centrifuged at 100,000 × g for 90 min using a Beckman Optima L-100 XP ultracentrifuge. The pellet containing exosomes was washed once with cold PBS and centrifuged again at 100,000 × g for 90 min using a Beckman optima MAX ultracentrifuge. Exosome pellets were either resuspended in 50 μl of RIPA buffer for Western blot analysis, or when treating primary microglia cells, they were resuspended in 150 μl of DMEM-F12. Total serum exosomes from welders and control subjects were isolated using ExoQuick (System Biosciences) reagent following the manufacturer's recommended protocol.

MTT assays

The 3-(4,5-dimethylthiazol-3-yl)-2,5-diphenyl tetrazolium bromide (MTT) assay has been widely used to assess the median lethal dose (LC_{50}) and cell viability by measuring the formazan produced when mitochondrial dehydrogenase enzymes cleave the tetrazolium ring (29). In this study, we used the MTT assay to determine the LC_{50} of Mn for MN9D cells. Briefly, 20,000 MN9D cells were seeded on a 96-well microplate, allowed to adhere for 16 h, and then treated for 24 hours with Mn (0 to 10 mM) in serum-free DMEM media. Following the treatment, the cells were washed with warm PBS and then incubated with 200 μl 0.25% (w/v) MTT in serum-free DMEM for 2 hours at 37 °C. The supernatant was removed and MTT crystals were solubilized in 200 μl dimethyl sulfoxide (DMSO). Mitochondrial activity was measured with the SpectraMax spectrophotometer (Molecular Devices Corporation) at 570 nm with the reference wavelength at 630 nm.

Nitric oxide and cytokine detection in microglia

Quantification of nitric oxide production by microglial cells after exosome treatment was measured indirectly by quantification of nitrite in the supernatant using the Griess reagent (Sigma Aldrich). Microglia plated at 70,000 cells/well were either treated for 24 hours with exosomes (1:100), or pretreated with endocytosis inhibitors for one hour and co-treated with exosomes for 24 h. At the end of treatments, equal volumes of cell media and Griess reagent were added to a 96-well plate along with a sodium nitrite standard curve, and absorbance at 540 nm was measured on a SpectraMax microplate reader. The supernatant was used to determine extracellular cytokine levels using the Luminex bead-based immunoassay system and recombinant standards for IL-6, IL-12, IL-10, TNF-α, and IL-1β (90).

Nanoparticle tracking analysis (NTA)

Ultracentrifuged or ExoQuick/TC-precipitated exosome samples were used for NTA, as previously described (12, 98, 99). Briefly, isolated exosomes were resuspended in 500–1000 μl PBS, from which approximately 300 μl was loaded into the sample chamber of an LM10 unit (NanoSight, Amesbury, UK) using a disposable syringe. Sample durations of 30–60 sec per sample were analyzed with NTA 2.3 software (NanoSight). Samples containing higher numbers of exosomes were diluted before the analysis and their relative concentrations then were calculated according to the dilution factor.

Transmission electron microscopy (TEM)

Purified exosomes were resuspended in 200 μl PBS. Next, 20 μl of each sample was mixed with uranyl acetate 2% (w/v) and incubated for 5 min, and then 5 μl were applied to carbon-coated copper grids. Images were taken using a JEOL 2100 200 kV scanning and transmission electron microscope (STEM) with a Thermo Fisher Noran System 6 elemental analysis system. TEM was operated at 80 kV and images were obtained at 18000–20000× magnification.

Quantification of αSyn in exosomes

Concentrations of αSyn in cell-derived exosomes and human exosomes isolated from serum were determined by using human αSyn ELISA kits (Invitrogen, Cat# KHB0061 and

Covance, Cat# SIG-38974), as previously described (100). Briefly, exosomes were isolated using ultracentrifugation or by ExoQuick reagent and lysed using RIPA buffer following manufacturer's instructions.

αSyn fibril formation assays

For the αSyn amyloid fibrillization assay, purified recombinant non-aggregated human αSyn was used as a substrate, and exosomes isolated from welder and control serum samples were used as a seed. The assay also consisted of blank (PBS) wells as a negative control and exogenously produced recombinant αSyn fibrils as a positive control. Each sample was run in 4 replicates and the representative graph shown for welders and controls consists of average fluorescence from all welders and controls with 4 replicates for each sample. The αSyn fibrillization assay was performed in a 100-μl reaction mixture consisting of 5 μl of 100-fold diluted serum exosomes in 0.05% SDS in PBS, 0.2 mg/ml recombinant αSyn, 300 mM NaCl, 10 μM EDTA, and 20 μM Thioflavin-T in a BMG CLARIOstar® plate reader using Nunc™ MicroWell™ 96-well optical-bottom plates. The reaction was carried out at 37°C by alternating shake and rest cycles every other minute with readings taken every 30 min over a 60-h period.

Animal studies

Male C57BL/6 mice (8–12 weeks old) were purchased from Charles River Laboratories and used for all mouse experiments. Human αSyn-A53T-overexpressing BAC transgenic rats (model number 10678) and non-carrier littermate control Sprague Dawley rats were obtained from Taconic Biosciences (Germantown, NY). Rodents were housed on a 12-h light cycle with *ad libitum* access to food and water. Iowa State University's (ISU) laboratory animal facility is fully accredited by the Association for Assessment and Accreditation of Laboratory Animal Care (AAALAC), and all procedures involving animal handling were approved by the Institutional Animal Care and Use Committee (IACUC) at ISU. For unilateral viral transduction experiments in mice, we injected a total volume of 2 μl of virus at a rate of 0.2 μl/min using a 10-μl Hamilton syringe with a 30-gauge needle, which was guided using the Angle 2 stereotaxic apparatus (Leica Biosystems, St. Louis, MO) to target the SN with the use of the following coordinates (mm from bregma): AP −3.30, ML −1.20 and DV −4.60. For co-transduction of AAV8_V1S and AAV8_SV2 viruses, 1 μl of pAAV8-CBA-Venus1-Synuclein-WPRE (AAV8_V1S) virus (titer 8.3×10^{12} viral genome/ml) and 1 μl of pAAV8-CBA-Synuclein-Venus2-WPRE (AAV8_SV2) virus (titer 8.7×10^{12} viral genome/ml) were injected. For the VenusYFP transduction group, 2 μl of pAAV8-CBA-Venus virus (titer 1×10^{12} viral genome/ml) was injected. Four weeks post-injection, the AAV8_V1S/AAV8_SV2 co-transduction group received either 15 mg/kg body weight/day Mn (as $MnCl_2$) for 30 days or an equal volume of vehicle (water) via oral gavage to assess the impact of environmental Mn exposure on the cell-to-cell transmission of αSyn. To control for the unintended effect of stereotaxic injections on animals, we also included a group of animals receiving 15 mg/kg Mn or an equal volume of vehicle, similar to the AAV co-transduction group, but without stereotaxic injection. To evaluate the effect of Mn on serum exosome numbers, human αSyn-A53T-overexpressing and non-transgenic rats were exposed to a similar Mn treatment paradigm as described for mice. This Mn dose regimen was chosen based on previous studies in humans and animals (72–74).

For stereotaxic delivery of exosomes to the striatum, we injected a total volume of 3 μl of exosomes (3.6×10^8 particle numbers) isolated from Mn- or vehicle-stimulated GFP_Syn and GFP_EV cells. Twelve weeks post-injection, animals were subjected to a battery of behavior tests, including an open-field test and the amphetamine-induced rotational test. Mice then were sacrificed and their tissues collected for biochemical and neurochemical analyses, or they were transcardially perfused for histological procedures.

Behavioral measurements

Exploratory locomotor activity was measured using the VersaMax open-field apparatus (AccuScan Instruments, Columbus, OH) as described previously (96) and the following indices were monitored for 10 min: rearing activity (labeled as vertical activity), horizontal activity, total distance traveled, stereotypy count and total movement time. The rotameter test was used to assess the effects of unilateral exosome injection-induced lesions. At 160 days post-exosome injection, mice received 5 mg/kg amphetamine (D-amphetamine sulphate, Sigma) intraperitoneally. Then after 20 min, each mouse was placed in a cylindrical bowl within which amphetamine-induced ipsilateral rotation was recorded via a video-camera coupled to automated tracking software (ANY-maze, Stoelting). Rotational scores were used as an estimate of the extent of lesions with data expressed as the average numbers of ipsilateral rotations per 20-min period.

Human studies

Sixty-six subjects were recruited initially from meetings of regional unions in Philadelphia and Harrisburg, Pennsylvania, and from the community around the Penn State Milton S. Hershey Medical Center. Welders (45.8 ± 11.2 years old) were defined as subjects with recent exposure (within 90 days), and controls as those without a history of welding. All subjects were male, answered negatively for past Parkinson's diagnosis or other neurological disorders, and were free of any obvious neurological or movement deficits using the Unified Parkinson's Disease Rating Scale (UPDRS-III) with a threshold score of <15 (24). For detailed demographic information, including exposure metrics, blood metal levels and MRI measures [(R1 regional values and pallidal index (PI)] in welder and control cohorts, please refer to our previous publications (101, 102). Written informed consent was obtained in accordance with guidelines approved by the Penn State Hershey Internal Review Board. Welders represented several trades and industry groups (such as boilermakers, pipefitters, railroad welders, and various manufacturing jobs). Controls were age-matched volunteers from the same regional community with various occupations. Whole blood samples were obtained by venipuncture. Samples rested at room temperature for ~15 min, after which they were centrifuged. The serum supernatant was pipetted in 1 mL aliquots into 2.5 mL cryovials and stored at −80° C. Prior to sending samples to Iowa State, samples were blinded and 200 μL of serum was shipped overnight. This serum was used to isolate exosomes as described above and was analyzed for exosome numbers, total αSyn concentration using ELISA, and misfolded αSyn content using αSyn amyloid fibrillization assay. These "blinded" samples were analyzed and exosome numbers were reported back to Penn State for unblinding and further analysis.

Statistical analysis

Data analysis was performed using Prism 7.0 software (GraphPad). Normally distributed raw data were analyzed with either Student's t-test or using one-way ANOVA, and then Tukey's post-test was performed to compare all treatment groups. Raw data from non-Gaussian distributions were analyzed with Kruskal-Wallis test followed by Dunn's multiple comparison test to compare all treatment groups. Experiments compared the mean differences between all groups using three-way ANOVA followed by Tukey-Kramer multiple comparisons using SAS system. Statistically significant differences were denoted as *$p \leq 0.05$, **$p < 0.01$, and ***$p < 0.001$.

Supplementary Material

Refer to Web version on PubMed Central for supplementary material.

Acknowledgments:

The authors thank Michael Cho (Iowa State University) for use of ultracentrifuge and NanoSight instruments, Chi-Fu Yen for assistance in MATLAB data analysis, and Chong Wang (Department of Statistics, Iowa State University) for assistance with statistical analyses. We thank David Rubinsztein (Cambridge), Hilal Lashuel (Swiss Federal Institute of Technology-Lausanne), and Pamela J. McLean (Mayo Clinic) for the various plasmids; the Michael J. Fox Foundation for Parkinson's Research for gifting us the recombinant αSyn monomers and fibrils; Douglas Golenbock (University of Massachusetts Medical School) for the WTMC cell line. We also like to thank Margaret Carter at Iowa State University's Confocal Microscopy Facility for her assistance with confocal microscopy and Imaris image analysis software.

Funding:

This work was supported by National Institutes of Health R01 grants [ES026892, ES019267, and ES025991] to A.G.K. and NS088206 to A.K. The W. Eugene and Linda Lloyd Endowed Chair and Armbrust Endowment to A.G.K. and Syngenta Fellowship Award in Human Health Applications of New Technologies to D.S.H. are also acknowledged.

References and Notes

1. Rokad D et al., Role of neurotoxicants and traumatic brain injury in alpha-synuclein protein misfolding and aggregation. Brain research bulletin 133, 60–70 (2017). [PubMed: 27993598]
2. El-Agnaf OM et al., Alpha-synuclein implicated in Parkinson's disease is present in extracellular biological fluids, including human plasma. FASEB J 17, 1945–1947 (2003). [PubMed: 14519670]
3. Kordower JH, Chu Y, Hauser RA, Freeman TB, Olanow CW, Lewy body-like pathology in long-term embryonic nigral transplants in Parkinson's disease. Nat Med 14, 504–506 (2008). [PubMed: 18391962]
4. Li JY et al., Lewy bodies in grafted neurons in subjects with Parkinson's disease suggest host-to-graft disease propagation. Nat Med 14, 501–503 (2008). [PubMed: 18391963]
5. Bae EJ et al., Glucocerebrosidase depletion enhances cell-to-cell transmission of alpha-synuclein. Nature communications 5, 4755 (2014).
6. Danzer KM et al., Exosomal cell-to-cell transmission of alpha synuclein oligomers. Molecular neurodegeneration 7, 42 (2012). [PubMed: 22920859]
7. Lee SJ, Desplats P, Sigurdson C, Tsigelny I, Masliah E, Cell-to-cell transmission of non-prion protein aggregates. Nat Rev Neurol 6, 702–706 (2010). [PubMed: 21045796]
8. Prusiner SB et al., Evidence for alpha-synuclein prions causing multiple system atrophy in humans with parkinsonism. Proc Natl Acad Sci U S A 112, E5308–5317 (2015). [PubMed: 26324905]
9. Emmanouilidou E et al., Cell-produced alpha-synuclein is secreted in a calcium-dependent manner by exosomes and impacts neuronal survival. The Journal of neuroscience : the official journal of the Society for Neuroscience 30, 6838–6851 (2010). [PubMed: 20484626]

10. Su X et al., Synuclein activates microglia in a model of Parkinson's disease. Neurobiology of aging 29, 1690–1701 (2008). [PubMed: 17537546]
11. Lee HJ, Patel S, Lee SJ, Intravesicular localization and exocytosis of alpha-synuclein and its aggregates. The Journal of neuroscience : the official journal of the Society for Neuroscience 25, 6016–6024 (2005). [PubMed: 15976091]
12. Harischandra DS et al., Environmental neurotoxicant manganese regulates exosome-mediated extracellular miRNAs in cell culture model of Parkinson's disease: Relevance to alpha-synuclein misfolding in metal neurotoxicity. Neurotoxicology 64, 267–277 (2018). [PubMed: 28450057]
13. Harischandra DS, Ghaisas S, Rokad D, Kanthasamy AG, Exosomes in Toxicology: Relevance to Chemical Exposure and Pathogenesis of Environmentally Linked Diseases. Toxicol Sci 158, 3–13 (2017). [PubMed: 28505322]
14. Chen Z et al., Incorporation of therapeutically modified bacteria into gut microbiota inhibits obesity. J Clin Invest 124, 3391–3406 (2014). [PubMed: 24960158]
15. Luk KC et al., Pathological alpha-synuclein transmission initiates Parkinson-like neurodegeneration in nontransgenic mice. Science 338, 949–953 (2012). [PubMed: 23161999]
16. Luk KC et al., Exogenous alpha-synuclein fibrils seed the formation of Lewy body-like intracellular inclusions in cultured cells. Proc Natl Acad Sci U S A 106, 20051–20056 (2009). [PubMed: 19892735]
17. Volpicelli-Daley LA, Luk KC, Lee VM, Addition of exogenous alpha-synuclein preformed fibrils to primary neuronal cultures to seed recruitment of endogenous alpha-synuclein to Lewy body and Lewy neurite-like aggregates. Nat Protoc 9, 2135–2146 (2014). [PubMed: 25122523]
18. Volpicelli-Daley LA et al., Exogenous alpha-synuclein fibrils induce Lewy body pathology leading to synaptic dysfunction and neuron death. Neuron 72, 57–71 (2011). [PubMed: 21982369]
19. Goldman SM, Environmental toxins and Parkinson's disease. Annu Rev Pharmacol Toxicol 54, 141–164 (2014). [PubMed: 24050700]
20. Koller WC, Lyons KE, Truly W, Effect of levodopa treatment for parkinsonism in welders: A double-blind study. Neurology 62, 730–733 (2004). [PubMed: 15007122]
21. Gorell JM et al., Occupational exposures to metals as risk factors for Parkinson's disease. Neurology 48, 650–658 (1997). [PubMed: 9065542]
22. Lee EY et al., T1 Relaxation Rate (R1) Indicates Nonlinear Mn Accumulation in Brain Tissue of Welders With Low-Level Exposure. Toxicol Sci 146, 281–289 (2015). [PubMed: 25953701]
23. Lee EY et al., Increased R2* in the Caudate Nucleus of Asymptomatic Welders. Toxicol Sci 150, 369–377 (2016). [PubMed: 26769335]
24. Racette BA et al., Increased risk of parkinsonism associated with welding exposure. Neurotoxicology 33, 1356–1361 (2012). [PubMed: 22975422]
25. Desplats P et al., Inclusion formation and neuronal cell death through neuron-to-neuron transmission of alpha-synuclein. Proceedings of the National Academy of Sciences of the United States of America 106, 13010–13015 (2009). [PubMed: 19651612]
26. Hansen C et al., alpha-Synuclein propagates from mouse brain to grafted dopaminergic neurons and seeds aggregation in cultured human cells. The Journal of clinical investigation 121, 715–725 (2011). [PubMed: 21245577]
27. Visanji NP, Brooks PL, Hazrati LN, Lang AE, The prion hypothesis in Parkinson's disease: Braak to the future. Acta neuropathologica communications 1, 2 (2013). [PubMed: 24252164]
28. Cai T et al., Manganese induces the overexpression of alpha-synuclein in PC12 cells via ERK activation. Brain research 1359, 201–207 (2010). [PubMed: 20735995]
29. Latchoumycandane C et al., Protein kinase Cdelta is a key downstream mediator of manganese-induced apoptosis in dopaminergic neuronal cells. J Pharmacol Exp Ther 313, 46–55 (2005). [PubMed: 15608081]
30. Glabe CG, Structural classification of toxic amyloid oligomers. J Biol Chem 283, 29639–29643 (2008). [PubMed: 18723507]
31. Henderson DM et al., Quantitative assessment of prion infectivity in tissues and body fluids by real-time quaking-induced conversion. The Journal of general virology 96, 210–219 (2015). [PubMed: 25304654]

32. Meisl G et al., Differences in nucleation behavior underlie the contrasting aggregation kinetics of the Abeta40 and Abeta42 peptides. Proc Natl Acad Sci U S A 111, 9384–9389 (2014). [PubMed: 24938782]
33. Feng D et al., Cellular internalization of exosomes occurs through phagocytosis. Traffic 11, 675–687 (2010). [PubMed: 20136776]
34. Amor S, Puentes F, Baker D, van der Valk P, Inflammation in neurodegenerative diseases. Immunology 129, 154–169 (2010). [PubMed: 20561356]
35. Heppner FL, Ransohoff RM, Becher B, Immune attack: the role of inflammation in Alzheimer disease. Nat Rev Neurosci 16, 358–372 (2015). [PubMed: 25991443]
36. Gao HM et al., Neuroinflammation and alpha-synuclein dysfunction potentiate each other, driving chronic progression of neurodegeneration in a mouse model of Parkinson's disease. Environ Health Perspect 119, 807–814 (2011). [PubMed: 21245015]
37. Mulcahy LA, Pink RC, Carter DR, Routes and mechanisms of extracellular vesicle uptake. J Extracell Vesicles 3, (2014).
38. Tian T et al., Exosome uptake through clathrin-mediated endocytosis and macropinocytosis and mediating miR-21 delivery. J Biol Chem 289, 22258–22267 (2014). [PubMed: 24951588]
39. Halle A et al., The NALP3 inflammasome is involved in the innate immune response to amyloid-beta. Nature immunology 9, 857–865 (2008). [PubMed: 18604209]
40. Rejman J, Bragonzi A, Conese M, Role of clathrin- and caveolae-mediated endocytosis in gene transfer mediated by lipo- and polyplexes. Mol Ther 12, 468–474 (2005). [PubMed: 15963763]
41. Hansen SH, Sandvig K, van Deurs B, Molecules internalized by clathrin-independent endocytosis are delivered to endosomes containing transferrin receptors. J Cell Biol 123, 89–97 (1993). [PubMed: 8408209]
42. Scholz D et al., Rapid, complete and large-scale generation of post-mitotic neurons from the human LUHMES cell line. Journal of neurochemistry 119, 957–971 (2011). [PubMed: 21434924]
43. Dimant H et al., Direct detection of alpha synuclein oligomers in vivo. Acta neuropathologica communications 1, 6 (2013). [PubMed: 24252244]
44. Outeiro TF et al., Formation of toxic oligomeric alpha-synuclein species in living cells. PLoS One 3, e1867 (2008). [PubMed: 18382657]
45. Bioscience T, "Expression Analysis of Rats Genetically Modified to Express the Human Alpha-Synuclein Gene " (2012).
46. Luk KC et al., Intracerebral inoculation of pathological alpha-synuclein initiates a rapidly progressive neurodegenerative alpha-synucleinopathy in mice. The Journal of experimental medicine 209, 975–986 (2012). [PubMed: 22508839]
47. Guo JL, Lee VM, Cell-to-cell transmission of pathogenic proteins in neurodegenerative diseases. Nat Med 20, 130–138 (2014). [PubMed: 24504409]
48. Fored CM et al., Parkinson's disease and other basal ganglia or movement disorders in a large nationwide cohort of Swedish welders. Occup Environ Med 63, 135–140 (2006). [PubMed: 16421393]
49. Willis AW et al., Predictors of survival in patients with Parkinson disease. Arch Neurol 69, 601–607 (2012). [PubMed: 22213411]
50. Wright Willis A, Evanoff BA, Lian M, Criswell SR, Racette BA, Geographic and ethnic variation in Parkinson disease: a population-based study of US Medicare beneficiaries. Neuroepidemiology 34, 143–151 (2010). [PubMed: 20090375]
51. Guilarte TR, Manganese and Parkinson's disease: a critical review and new findings. Environmental health perspectives 118, 1071–1080 (2010). [PubMed: 20403794]
52. Foulds PG et al., Phosphorylated alpha-synuclein can be detected in blood plasma and is potentially a useful biomarker for Parkinson's disease. FASEB J 25, 4127–4137 (2011). [PubMed: 21865317]
53. Mollenhauer B et al., Total CSF alpha-synuclein is lower in de novo Parkinson patients than in healthy subjects. Neurosci Lett 532, 44–48 (2013). [PubMed: 23149132]
54. Sharon R et al., The formation of highly soluble oligomers of alpha-synuclein is regulated by fatty acids and enhanced in Parkinson's disease. Neuron 37, 583–595 (2003). [PubMed: 12597857]

55. Winner B et al., In vivo demonstration that alpha-synuclein oligomers are toxic. Proc Natl Acad Sci U S A 108, 4194–4199 (2011). [PubMed: 21325059]
56. Shi M et al., Plasma exosomal alpha-synuclein is likely CNS-derived and increased in Parkinson's disease. Acta Neuropathol 128, 639–650 (2014). [PubMed: 24997849]
57. Fiandaca MS et al., Identification of preclinical Alzheimer's disease by a profile of pathogenic proteins in neurally derived blood exosomes: A case-control study. Alzheimer's & dementia : the journal of the Alzheimer's Association 11, 600–607.e601 (2015).
58. Ubeda-Banon I, Saiz-Sanchez D, de la Rosa-Prieto C, Martinez-Marcos A, alpha-Synuclein in the olfactory system in Parkinson's disease: role of neural connections on spreading pathology. Brain structure & function, (2013).
59. Watts JC et al., Transmission of multiple system atrophy prions to transgenic mice. Proc Natl Acad Sci U S A 110, 19555–19560 (2013). [PubMed: 24218576]
60. Claassen DO et al., Cortical asymmetry in Parkinson's disease: early susceptibility of the left hemisphere. Brain Behav 6, e00573 (2016). [PubMed: 28031997]
61. Djaldetti R, Ziv I, Melamed E, The mystery of motor asymmetry in Parkinson's disease. Lancet Neurol 5, 796–802 (2006). [PubMed: 16914408]
62. Wang J et al., MRI evaluation of asymmetry of nigrostriatal damage in the early stage of early-onset Parkinson's disease. Parkinsonism Relat Disord 21, 590–596 (2015). [PubMed: 25825242]
63. Kim C et al., Neuron-released oligomeric alpha-synuclein is an endogenous agonist of TLR2 for paracrine activation of microglia. Nat Commun 4, 1562 (2013). [PubMed: 23463005]
64. Aguzzi A, Falsig J, Prion propagation, toxicity and degradation. Nat Neurosci 15, 936–939 (2012). [PubMed: 22735515]
65. Hirata Y, Manganese-induced apoptosis in PC12 cells. Neurotoxicol Teratol 24, 639–653 (2002). [PubMed: 12200195]
66. Horning KJ, Caito SW, Tipps KG, Bowman AB, Aschner M, Manganese Is Essential for Neuronal Health. Annu Rev Nutr 35, 71–108 (2015). [PubMed: 25974698]
67. Vekrellis K, Xilouri M, Emmanouilidou E, Rideout HJ, Stefanis L, Pathological roles of alpha-synuclein in neurological disorders. Lancet Neurol 10, 1015–1025 (2011). [PubMed: 22014436]
68. Schneider A, Simons M, Exosomes: vesicular carriers for intercellular communication in neurodegenerative disorders. Cell Tissue Res 352, 33–47 (2013). [PubMed: 22610588]
69. Alvarez-Erviti L et al., Lysosomal dysfunction increases exosome-mediated alpha-synuclein release and transmission. Neurobiology of disease 42, 360–367 (2011). [PubMed: 21303699]
70. Fellner L et al., Toll-like receptor 4 is required for alpha-synuclein dependent activation of microglia and astroglia. Glia 61, 349–360 (2013). [PubMed: 23108585]
71. Harischandra DS, Jin H, Anantharam V, Kanthasamy A, Kanthasamy AG, alpha-Synuclein protects against manganese neurotoxic insult during the early stages of exposure in a dopaminergic cell model of Parkinson's disease. Toxicol Sci 143, 454–468 (2015). [PubMed: 25416158]
72. Crossgrove J, Zheng W, Manganese toxicity upon overexposure. NMR Biomed 17, 544–553 (2004). [PubMed: 15617053]
73. Li GJ et al., Molecular mechanism of distorted iron regulation in the blood-CSF barrier and regional blood-brain barrier following in vivo subchronic manganese exposure. Neurotoxicology 27, 737–744 (2006). [PubMed: 16545456]
74. Zheng W, Kim H, Zhao Q, Comparative toxicokinetics of manganese chloride and methylcyclopentadienyl manganese tricarbonyl (MMT) in Sprague-Dawley rats. Toxicol Sci 54, 295–301 (2000). [PubMed: 10774811]
75. Peneder TM et al., Chronic exposure to manganese decreases striatal dopamine turnover in human alpha-synuclein transgenic mice. Neuroscience 180, 280–292 (2011). [PubMed: 21333719]
76. Foulds PG et al., A longitudinal study on alpha-synuclein in blood plasma as a biomarker for Parkinson's disease. Sci Rep 3, 2540 (2013). [PubMed: 23985836]
77. Sato H, Kato T, Arawaka S, The role of Ser129 phosphorylation of alpha-synuclein in neurodegeneration of Parkinson's disease: a review of in vivo models. Rev Neurosci 24, 115–123 (2013). [PubMed: 23314528]

78. Peelaerts W et al., alpha-Synuclein strains cause distinct synucleinopathies after local and systemic administration. Nature 522, 340–344 (2015). [PubMed: 26061766]

79. Sacino AN et al., Intramuscular injection of alpha-synuclein induces CNS alpha-synuclein pathology and a rapid-onset motor phenotype in transgenic mice. Proc Natl Acad Sci U S A 111, 10732–10737 (2014). [PubMed: 25002524]

80. Holmqvist S et al., Direct evidence of Parkinson pathology spread from the gastrointestinal tract to the brain in rats. Acta neuropathologica 128, 805–820 (2014). [PubMed: 25296989]

81. Alvarez-Erviti L et al., Delivery of siRNA to the mouse brain by systemic injection of targeted exosomes. Nat Biotechnol 29, 341–345 (2011). [PubMed: 21423189]

82. Cook C et al., Tau deposition drives neuropathological, inflammatory and behavioral abnormalities independently of neuronal loss in a novel mouse model. Hum Mol Genet 24, 6198–6212 (2015). [PubMed: 26276810]

83. Litvan I et al., Movement Disorders Society Scientific Issues Committee report: SIC Task Force appraisal of clinical diagnostic criteria for Parkinsonian disorders. Mov Disord 18, 467–486 (2003). [PubMed: 12722160]

84. Schwab C, Klegeris A, McGeer PL, Inflammation in transgenic mouse models of neurodegenerative disorders. Biochim Biophys Acta 1802, 889–902 (2010). [PubMed: 19883753]

85. Postuma RB et al., Quantifying the risk of neurodegenerative disease in idiopathic REM sleep behavior disorder. Neurology 72, 1296–1300 (2009). [PubMed: 19109537]

86. Tanaka S et al., Activation of microglia induces symptoms of Parkinson's disease in wild-type, but not in IL-1 knockout mice. J Neuroinflammation 10, 143 (2013). [PubMed: 24289537]

87. Wang Q, Liu Y, Zhou J, Neuroinflammation in Parkinson's disease and its potential as therapeutic target. Transl Neurodegener 4, 19 (2015). [PubMed: 26464797]

88. Furlong RA, Narain Y, Rankin J, Wyttenbach A, Rubinsztein DC, Alpha-synuclein overexpression promotes aggregation of mutant huntingtin. Biochem J 346 Pt 3, 577–581 (2000). [PubMed: 10698681]

89. Paleologou KE et al., Phosphorylation at Ser-129 but not the phosphomimics S129E/D inhibits the fibrillation of alpha-synuclein. The Journal of biological chemistry 283, 16895–16905 (2008). [PubMed: 18343814]

90. Gordon R et al., A simple magnetic separation method for high-yield isolation of pure primary microglia. J Neurosci Methods 194, 287–296 (2011). [PubMed: 21074565]

91. Ay M et al., Molecular cloning, epigenetic regulation, and functional characterization of Prkd1 gene promoter in dopaminergic cell culture models of Parkinson's disease. J Neurochem 135, 402–415 (2015). [PubMed: 26230914]

92. Jin H et al., Histone Hyperacetylation Upregulates PKCdelta in Dopaminergic Neurons to Induce Cell Death: Relevance to Epigenetic Mechanisms of Neurodegeneration in Parkinson's Disease. The Journal of biological chemistry, (2014).

93. Brenza TM et al., Neuronal protection against oxidative insult by polyanhydride nanoparticle-based mitochondria-targeted antioxidant therapy. Nanomedicine : nanotechnology, biology, and medicine 13, 809–820 (2017).

94. Ghosh A et al., The peptidyl-prolyl isomerase Pin1 up-regulation and proapoptotic function in dopaminergic neurons: relevance to the pathogenesis of Parkinson disease. J Biol Chem 288, 21955–21971 (2013). [PubMed: 23754278]

95. Gordon R et al., Prokineticin-2 upregulation during neuronal injury mediates a compensatory protective response against dopaminergic neuronal degeneration. Nat Commun 7, 12932 (2016). [PubMed: 27703142]

96. Ghosh A et al., Neuroprotection by a mitochondria-targeted drug in a Parkinson's disease model. Free Radic Biol Med 49, 1674–1684 (2010). [PubMed: 20828611]

97. Harischandra DS et al., Role of proteolytic activation of protein kinase Cdelta in the pathogenesis of prion disease. Prion 8, 143–153 (2014). [PubMed: 24576946]

98. Soo CY et al., Nanoparticle tracking analysis monitors microvesicle and exosome secretion from immune cells. Immunology 136, 192–197 (2012). [PubMed: 22348503]

99. Harischandra H, Yuan W, Loghry HJ, Zamanian M, Kimber MJ, Profiling extracellular vesicle release by the filarial nematode Brugia malayi reveals sex-specific differences in cargo and a

sensitivity to ivermectin. PLoS neglected tropical diseases 12, e0006438 (2018). [PubMed: 29659599]

100. Wennstrom M, Londos E, Minthon L, Nielsen HM, Altered CSF orexin and alpha-synuclein levels in dementia patients. J Alzheimers Dis 29, 125–132 (2012). [PubMed: 22207004]
101. Lee E-Y et al., T1 relaxation rate (R1) indicates non-linear Mn accumulation in brain tissue of welders with low-level exposure. Toxicological Sciences, kfv088 (2015).
102. Lee EY et al., Association of neurobehavioral performance with R2* in the caudate nucleus of asymptomatic welders. Neurotoxicology 58, 66–74 (2017). [PubMed: 27871916]

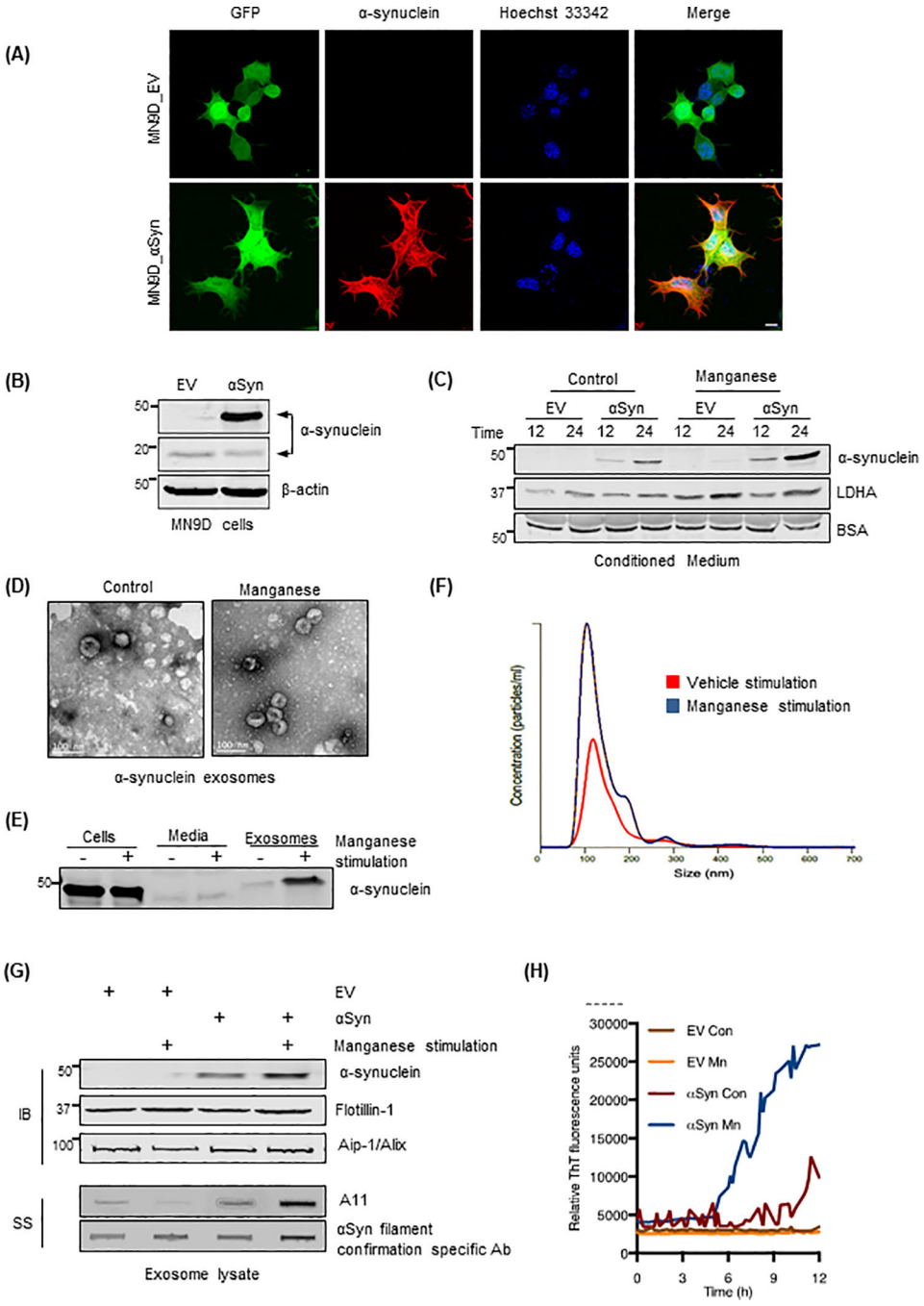

Figure 1: Mn upregulates exosomal release of oligomeric αSyn.

(A) Immunofluorescence of stably expressed GFP-fused human αSyn (red) in GFP_Syn M9ND cells and GFP fluorescence (green) in both control GFP_EV and human αSyn-expressing GFP_Syn cells. Hoechst dye stained the nuclei (blue). Magnification, 60X. Scale bar, 10 μm. **(B)** Western blots (WBs) of GFP_Syn and GFP_EV cells for human αSyn (~45 kDa) in GFP_Syn cells and endogenous mouse αSyn (18 kDa). **(C)** Representative WBs of conditioned medium from cells in (B), control or exposed to Mn (300 μM), for GFP-fused αSyn and LDHA. **(D)** TEM to examine the morphology of secreted exosomes from

GFP_Syn cells. Scale bar, 100 nm. **(E)** Western blot analysis for αSyn abundance in MN9D cells, conditioned media and exosomes. **(F)** Representative NanoSight Particle tracking, indicating size and concentration of exosomes from GFP_Syn cells, from vehicle-stimulated (red) and Mn-stimulated (blue) cells. **(G)** WBs for GFP-fused human αSyn in exosomes from GFP_Syn and GFP_EV cells. Exosome-positive markers flotillin-1 and Aip-1/Alix were enriched in both cell types. Slot blotting (SS) of exosome lysates indicates A11-positive oligomeric proteins and fibrillar αSyn in Mn-stimulated exosomes. **(H)** RT-QuIC of Mn-stimulated or vehicle-stimulated exosomes from GFP_Syn and GFP_EV cells to assess the abundance of misfolded αSyn.

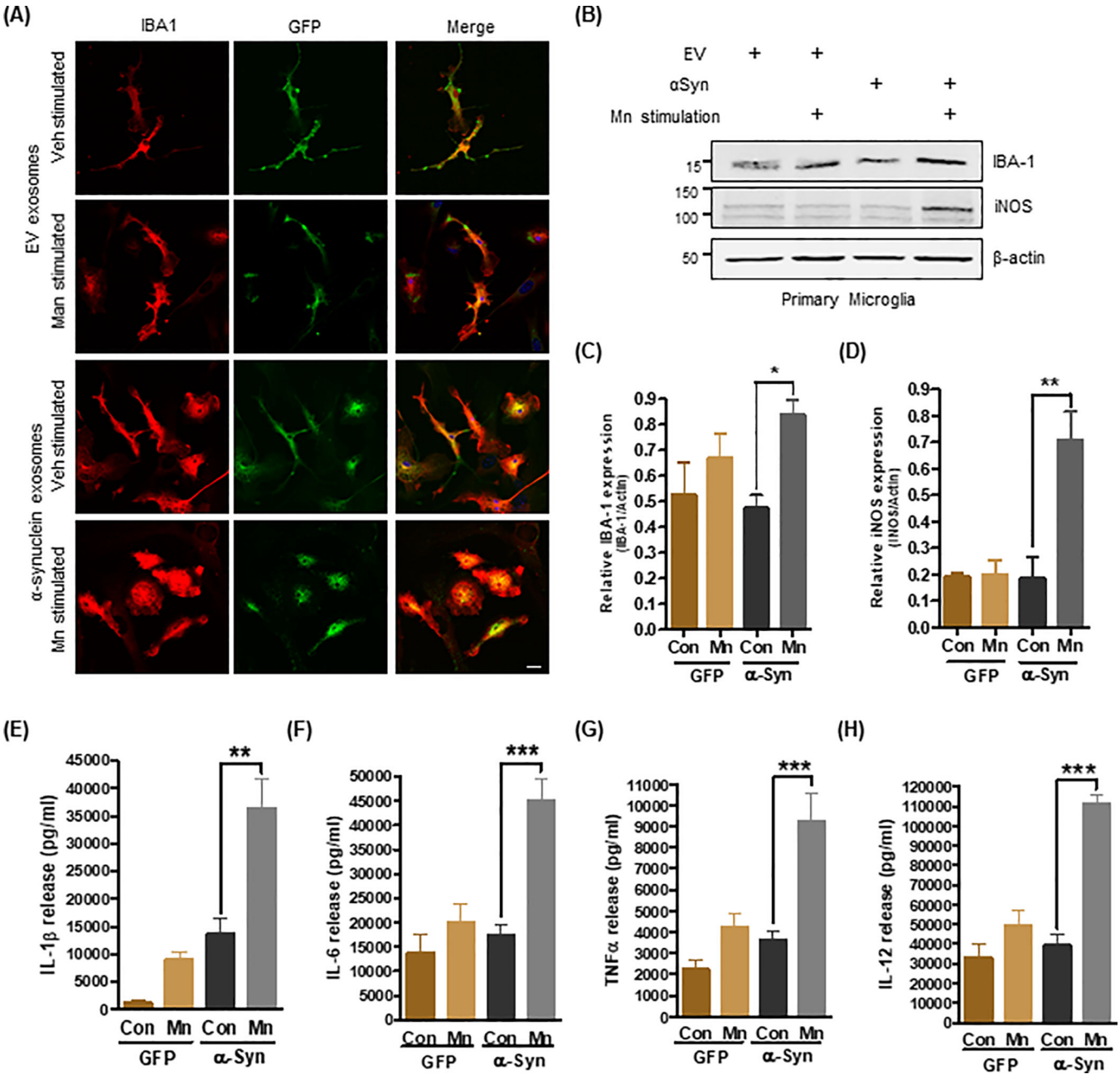

Figure 2: Mn-stimulated exosomes promote neuroinflammatory responses.

(A) Immunofluorescence analysis of primary microglial cells (IBA1; red color) exposed to exosomes (GFP; green color). Hoechst dye stained the nuclei (blue). Magnification, 60X; scale bar, 10 μm. Amoeboid and pseudopodic morphology of primary microglial cells exposed to Mn-stimulated αSyn exosomes was visually assessed (lower images). **(B to D)** Representative Western blots (B) and densitometry (C and D) assessing IBA-1 and iNOS abundance after exposure to Mn-stimulated αSyn exosomes, as a measure of their potential to promote neuroinflammatory responses in vitro. Data are mean ± SEM (*p≤0.05, **p<0.01 by one-way ANOVA with Tukey's post-test) of five independent experiments. **(E to H)** Pro-inflammatory cytokine release upon exosome treatment was quantified using

Luminex bead-based cytokine assays. Data are mean ± SEM (**p<0.01, ***p<0.001 by one-way ANOVA with Tukey's post-test) of four individual experiments performed in 8 replicates.

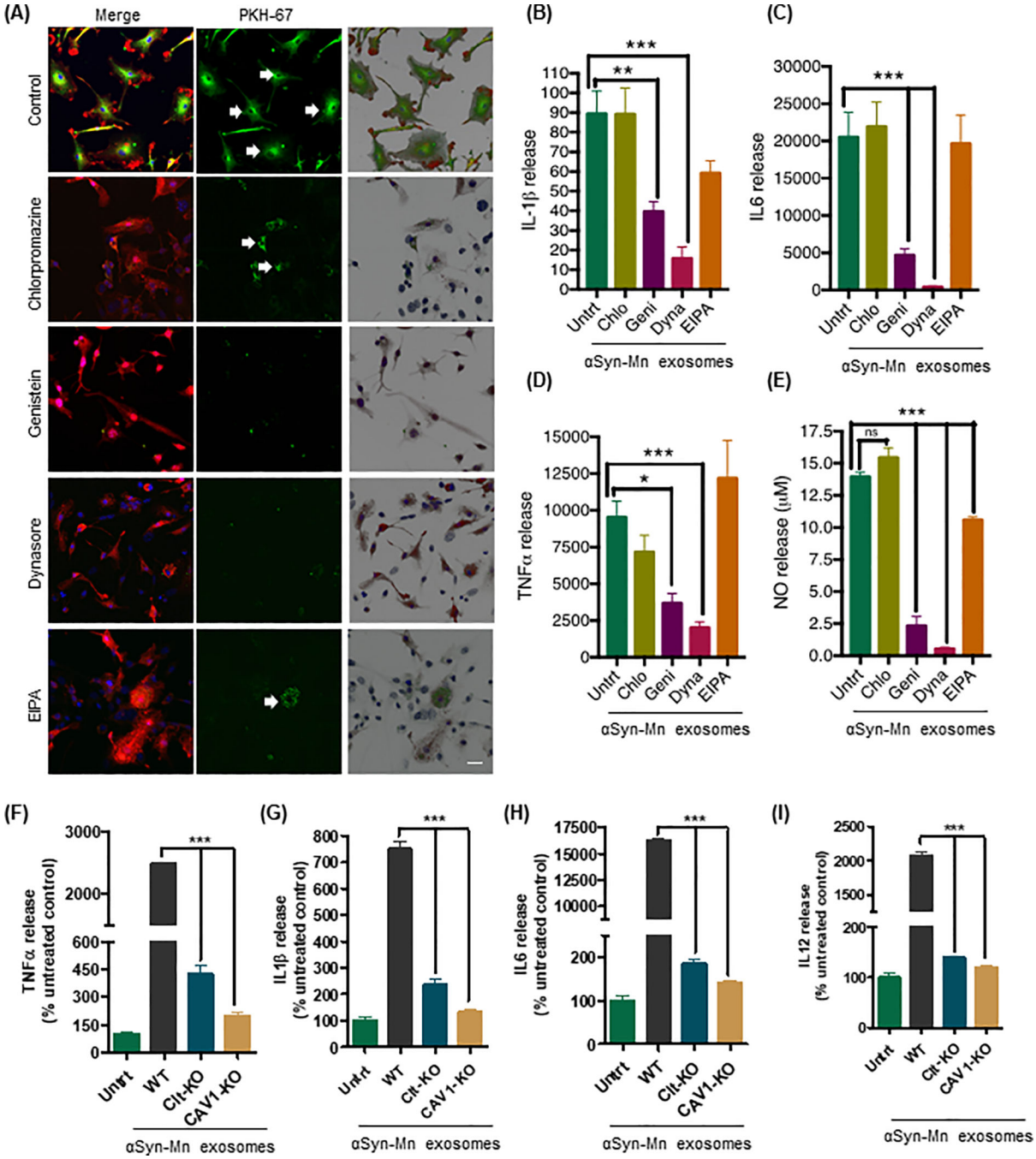

Figure 3: Microglia internalize Mn-stimulated αSyn exosomes through caveolin-1-mediated endocytosis.

(A) Immunofluorescence analysis of the chemical inhibition of Mn-stimulated αSyn exosome uptake. The left column represents merged images of IBA-1 immuno-positive microglia (red) and PKH67-labeled exosomes (green), middle column represents effective uptake/inhibition of PKH67-labeled exosomes (green), and the right column represents the 3D surface reconstruction generated by Imaris software. Magnification, 60X. Scale bar, 10 μm. **(B to D)** Inhibition of pro-inflammatory cytokine release quantified using Luminex

bead-based cytokine assays. Data are mean ± SEM (*p≤0.05, **p<0.01, ***p<0.001 by one-way ANOVA with Tukey's post-test) of four individual experiments each performed with 8 technical replicates. **(E)** Effective inhibition of nitric oxide release from genistein and Dynasore (each 50 μM)-treated WTMC cells observed through Griess assay. Data are mean ± SEM (***p<0.001, ns = not significant) of four individual experiments performed in 8 replicates. **(F to I)** Assessment of pro-inflammatory cytokine release upon treatment of caveolin-1– or clathrin–knockdown (Cav1-KD and CLTC-KD, respectively) primary murine microglial cells with Mn-stimulated αSyn exosomes, quantified using Luminex bead-based cytokine assay. Data are mean ± SEM (**p<0.01, ***p<0.001 by one-way ANOVA with Tukey's post-test) of four individual experiments performed in 8 replicates.

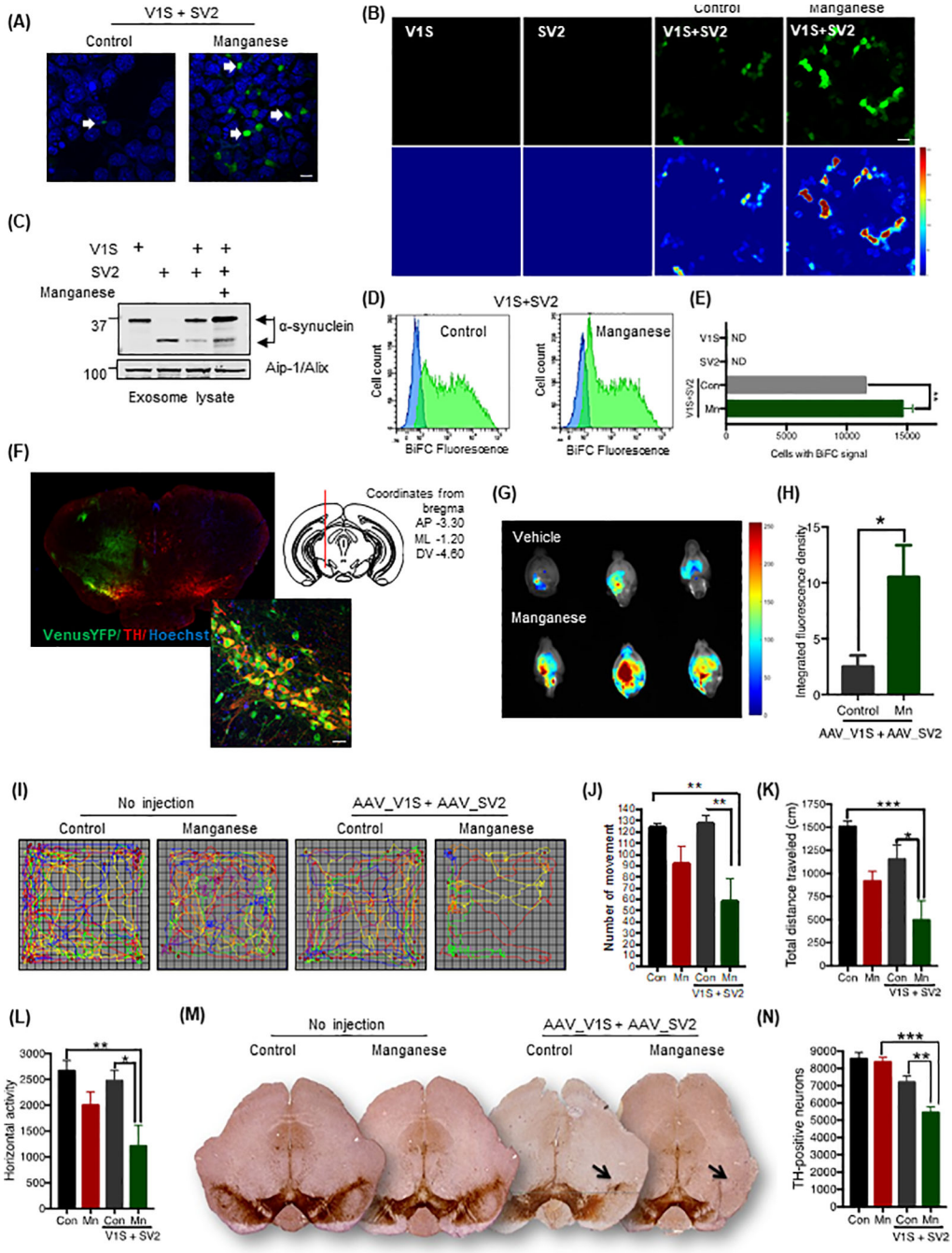

Figure 4: Mn-induced cell-to-cell transmission of αSyn oligomers.

(A and B) Confocal microscopy assessing BiFC for control and Mn-treated V1S/SV2 co-cultures. Magnification, 60X; scale bar, 10 μm. As a control, cells transfected with V1S-alone and SV2-alone (B) did not fluoresce. **(C)** Exosomal αSyn abundance detected in the conditioned media from V1S/SV2 co-cultures. **(D)** Representative FACS scatter plots assessing BiFC-positive cells in vehicle- and Mn-treated S1V/SV2 co-transfection. **(E)** FACS analysis of BiFC-positive cells transfected with S1V, SV2, or both in control and Mn-treated cultures. Data are mean ± SEM of four experiments performed in duplicates;

p<0.01 by one-way ANOVA with Tukey's post-test. **(F) VenusYFP epifluorescence in SNpc. VenusYFP fluorescence (green, high-magnification inset) colocalized with SNpc TH-immunostaining (red). Hoechst dye stained nuclei (blue). Magnification, 60X; scale bar, 10 μm. Diagram illustrates injection (mm from bregma) of AAV8-V1S and AAV8-SV2. **(G)** Highest VenusYFP epifluorescence in Mn-exposed animals, localized via BiFC epifluorescence overlay. **(H)** Increased BiFC fluorescence in Mn-exposed mice. Data are mean ± SEM from 7 animals/group; *p≤0.05 by Student's t-test. **(I to K)** Representative movement tracks (I), number of movements (J), and total distance traveled (K) of control and Mn-exposed mice. Data are mean ± SEM of ≥12 animals per group; *p≤0.05, **p<0.01, and ***p<0.001 by one-way ANOVA with Tukey's post-test. **(L and M)** DAB-based detection (L) and stereological counting (K) of TH-positive neurons in coronal SNpc sections from control and Mn-exposed mice. Images (L) are representative, at 2X magnification; arrows indicate loss of TH-positive neurons in Mn-treated mice. Data (M) are mean ± SEM from 7 animals per group; **p<0.01 and ***p<0.001 by one-way ANOVA with Tukey's post-test. **(N)** Horizontal activity of the mice described and analyzed in (I to K).

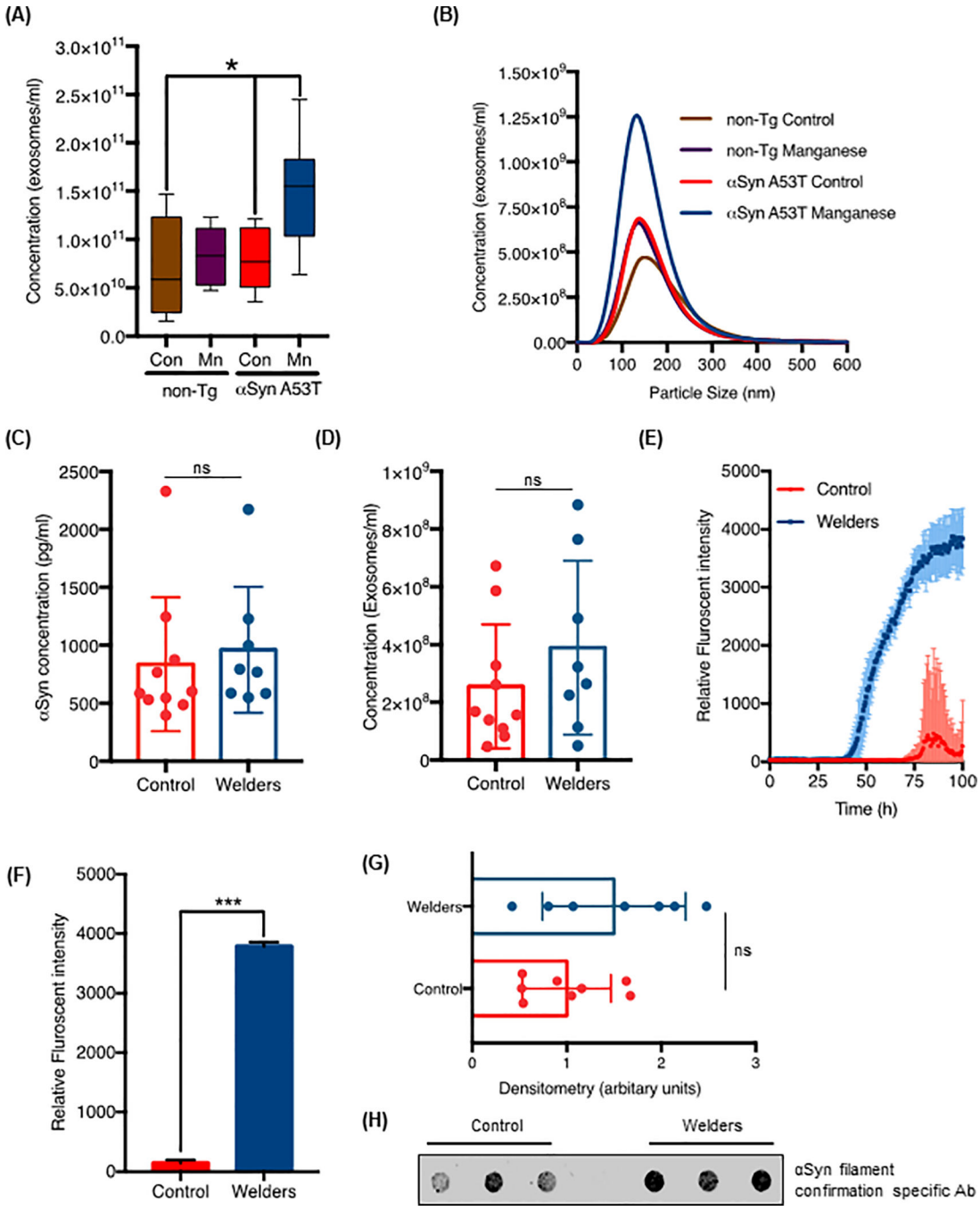

Figure 5: Mn exposure promotes exosome release in αSyn-A53T transgenic animals and αSyn oligomer transmission in humans.

(A and B) Concentration (A) and representative NanoSight Particle tracking size distribution plot (B) of serum exosomes isolated from αSyn-A53T transgenic and WT rats exposed to Mn (15 mg/kg body weight per day) or vehicle for 30 days (n = 7 rats per group). *p≤0.05 by Kruskal-Wallis with Dunn's multiple comparison test. **(C and D)** Scatter plots of total serum αSyn concentration (C) and total serum exosome concentration (D) measured by αSyn ELISA and NanoSight, respectively (ns = not significant; $P = 0.2855$ and 0.6472,

by Student's t-test, respectively). Data are mean ± SEM of 8 welders and 10 control human samples. **(E and F)** RT-QuIC assay comparing exosomes isolated from welders and control humans. Blue and red shaded areas (E) represent SEM of the mean ThT fluorescence for welder and control samples; (F) analysis of relative mean ThT fluorescence intensity in the groups. Data are from n= 10 samples per group; ***$p<0.001$ by Student's t-test **(G and H)** Scatter plots (G) of the densitometry analysis of the dot blots (H) assessing misfolded αSyn content in welder-derived and control individual-derived serum exosomes. Data are mean ± SEM of $n \geq 7$ samples each; ns = not significant by Student's t-test.

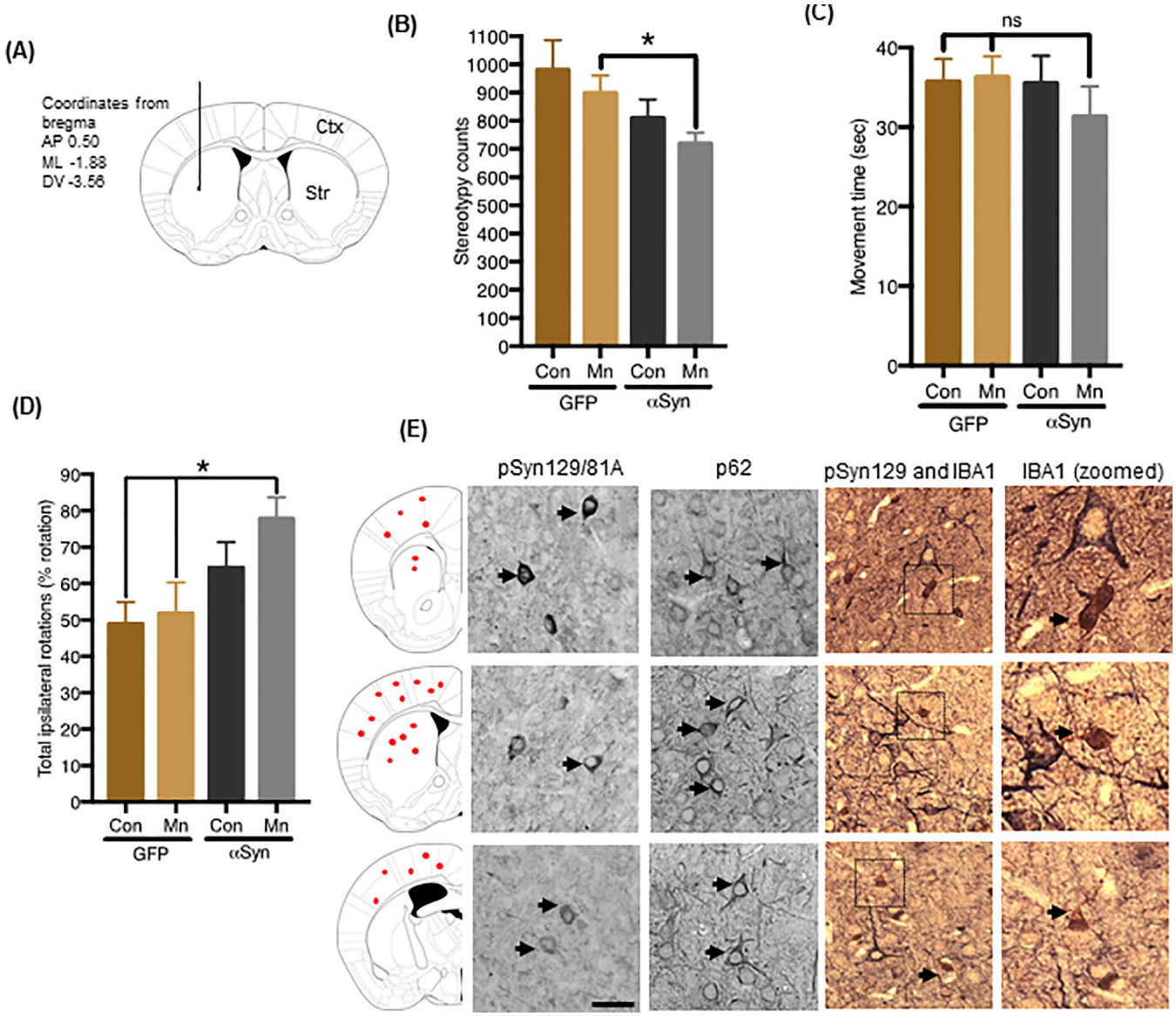

Figure 6: Mn-stimulated αSyn exosomes induce Parkinson-like motor deficits in non-transgenic mice.

(A) Diagram illustrating route and coordinates (mm from bregma) of stereotaxic exosome injections (coronal view). Exosomes were inoculated into the left hemisphere at subdural depths, indicated using a single needle tract. **(B and C)** Open-field behavior analysis measured using VersaMax apparatus, assessing stereotypy counts (B) and movement time (C) in C57BL/6 mice injected with exosomes isolated from Mn- or vehicle-treated GFP_EV and GFP_Syn cells. Data are mean ± SEM of n ≥12 animals per group; *p≤0.05; ns = not significant by one-way ANOVA with Tukey's post-test. **(D)** Immunohistological analysis of phosphorylated αSyn (pSyn129/81A), p62 immunoreactivity, and primary microglial cells (IBA1) in brain tissue from mice injected with Mn-stimulated αSyn exosomes. Corresponding brain regions shown in far-left panel. Magnification, 40X; scale bar, 25 μm. **(E)** Amphetamine-induced rotation test. The graph shows net scores for ipsilateral rotational

asymmetry (number and direction of rotations) induced by amphetamine 180 days post-lesioning in mice receiving vehicle- or Mn-stimulated GFP or αSyn exosomes.